

Warped Extra Dimensional Benchmarks for Snowmass 2013

Kaustubh Agashe^a, Oleg Antipin^b, Mihailo Backović^c, Aaron Effron^d, Alex Emerman^e,
Johannes Erdmann^d, Tobias Golling^d, Shrihari Gopalakrishna^f, Tuomas Hapola^g,
Shih-Chieh Hsu^h, José Juknevič^c, Seung J. Lee^{i,j}, Tanumoy Mandal^f, August Miller^k,
Edward Moyse^k, Tuhin Subhra Mukherjee^f, Chris Pollard^l, Soumya Sadhukhan^f, Daniel
Whiteson^m, Stephane Willocq^k

^a*Maryland Center for Fundamental Physics, Department of Physics, University of Maryland,
College Park, MD 20742, U.S.A.*

^b*CP³–Origins & the Danish Institute for Advanced Study Danish IAS, University of Southern
Denmark, Campusvej 55, DK-5230 Odense M, Denmark.*

^c*Department of Particle Physics and Astrophysics, Weizmann Institute of Science,
Rehovot 76100, Israel*

^d*Department of Physics, Yale University, New Haven, CT 06520, U.S.A.*

^e*Department of Physics, Reed College, Portland, OR 97202, U.S.A.*

^f*Institute of Mathematical Sciences (IMSc), C.I.T Campus, Taramani, Chennai 600113, India*

^g*Institute for Particle Physics Phenomenology, Durham University,
South Rd, Durham DH1 3LE, UK*

^h*Department of Physics, University of Washington Seattle, Seattle, WA 98195, U.S.A.*

ⁱ*Department of Physics, Korea Advanced Institute of Science and Technology,
335 Gwahak-ro, Yuseong-gu, Daejeon 305-701, Korea*

^j*School of Physics, Korea Institute for Advanced Study, Seoul 130-722, Korea*

^k*Department of Physics, University of Massachusetts, Amherst, MA 01003, U.S.A.*

^l*Department of Physics, Duke University, Durham, NC 27708, U.S.A.*

^m*Department of Physics and Astronomy, University of California, Irvine, CA 92697, U.S.A.*

Abstract

The framework of a warped extra dimension with the Standard Model (SM) fields propagating in it is a very well-motivated extension of the SM since it can address both the Planck-weak and flavor hierarchy problems of the SM. We consider signals at the 14 and 33 TeV large hadron collider (LHC) resulting from the direct production of the new particles in this framework, i.e., Kaluza-Klein (KK) excitations of the SM particles. We focus on spin-1 (gauge boson) and spin-2 (graviton) KK particles and their decays to top/bottom quarks (flavor-conserving) and W/Z and Higgs bosons, in particular. We propose two benchmarks for this purpose, with the right-handed (RH) or LH top quark, respectively, being localized very close to the TeV end of the extra dimension. We present some new results at the 14 TeV (with 300 fb⁻¹ and 3000 fb⁻¹) and 33 TeV LHC. We find that the prospects for discovery of these particles are quite promising, especially at the high-luminosity upgrade.

1 Introduction

The framework of a warped extra dimension a la Randall-Sundrum (RS1) model [1], but with all the SM fields propagating in it [2, 3, 4] is a very-well motivated extension of the Standard Model (SM): for a review and further references¹, see [6]. Such a framework can address both the Planck-weak and the flavor hierarchy problems of the SM, the latter without resulting in (at least a severe) flavor problem. The versions of this framework with a grand unified theory (GUT) in the bulk can naturally lead to precision unification of the three SM gauge couplings [7] and a candidate for the dark matter of the universe (the latter from requiring longevity of the proton) [8]. The new particles in this framework are Kaluza-Klein (KK) excitations of all SM fields with masses at $\sim \text{TeV}$ scale. In this write-up, we outline and suggest some benchmarks for the signals at the large hadron collider (LHC) for these new particles.

2 Review of Warped Extra Dimension

The framework consists of a slice of anti-de Sitter space in five dimensions (AdS_5), where (due to the warped geometry) the effective $4D$ mass scale is dependent on the position in the extra dimension. The $4D$ graviton, i.e., the zero-mode of the $5D$ graviton, is automatically localized at one end of the extra dimension (called the Planck/UV brane). If the Higgs sector is localized at the other end², then the warped geometry naturally generates the Planck-weak hierarchy. Specifically, we have $\text{TeV} \sim \bar{M}_P e^{-k\pi r_c}$, where \bar{M}_P is the reduced $4D$ Planck scale, k is the AdS_5 curvature scale and r_c is the proper size of the extra dimension. The crucial point is that the required modest size of the radius (in units of the curvature radius), i.e., $kr_c \sim 1/\pi \log(\bar{M}_P/\text{TeV}) \sim 10$ can be stabilized with only a corresponding modest tuning in the fundamental or $5D$ parameters of the theory [10]. Remarkably, the correspondence between AdS_5 and $4D$ conformal field theories (CFT) [11] suggests that the scenario with warped extra dimension is dual to the idea of a composite Higgs in $4D$ [9, 12].

2.1 SM in warped bulk

It was realized that with SM fermions propagating in the extra dimension, we can also account for the hierarchy between quark and lepton masses and mixing angles (flavor hierarchy) as follows [3, 4]: the basic idea is that the $4D$ Yukawa coupling are given by the product of the $5D$ Yukawa coupling and the overlap of the profiles in the extra dimension of the SM fermions (which are the zero-modes of the $5D$ fermions) with that of the Higgs. In turn, these fermion profiles are determined by $5D$ mass parameters, in units of k (denoted by c). The crucial point is that vastly different profiles for zero-mode fermions can be realized with small variations in the $5D$ mass parameters of fermions. So,

- the light SM fermions [i.e., 1st and 2nd generations and tau lepton and its neutrino, right-handed (RH) bottom quark] can be chosen to be localized near the Planck brane (via $c \gtrsim 1/2$), resulting in a small overlap with the TeV-brane localized SM Higgs, while the top quark [including possibly left-handed (LH) bottom quark, being the weak isospin partner of the LH top quark] is localized near the TeV brane ($c \lesssim 0$) with a large overlap with the Higgs.

¹i.e., the list of references given in this note is *not* meant to be complete or fully updated: we apologize in advance for this!

²In fact with SM Higgs originating as 5th component of a $5D$ gauge field (A_5) it is automatically so [9].

Thus we can obtain hierarchical SM Yukawa couplings without any large hierarchies in the parameters of the $5D$ theory, i.e. the $5D$ Yukawas and the $5D$ masses.³

With SM fermions emerging as zero-modes of $5D$ fermions, so must the SM gauge fields. Hence, this scenario can be dubbed “SM in the (warped) bulk”. Due to the different profiles of the SM fermions in the extra dimension, flavor changing neutral currents (FCNC) are generated by their non-universal couplings to gauge KK states. However, these contributions to the FCNC’s are suppressed due to an analog of the Glashow-Iliopoulos-Maiani (GIM) mechanism of the SM, i.e. RS-GIM, which is “built-in” [4, 14]. The point is that *all* KK modes (whether gauge, graviton or fermion) are localized near the TeV or IR brane (just like the Higgs) so that non-universalities in their couplings to SM fermions are of same size as couplings to the Higgs. In spite of this RS-GIM suppression, the lower limit on the KK mass scale can be ~ 10 TeV, although these constraints can be ameliorated by addition of flavor symmetries [15]. Finally, various custodial symmetries [16, 17] can be incorporated such that the constraints from the various (flavor-preserving) electroweak precision tests (EWPT) can be satisfied for a few TeV KK scale [18]. The bottom line is that a few TeV mass scale for the KK gauge bosons can be consistent with both electroweak and flavor precision tests.

2.2 Couplings of KK’s

Clearly, the light fermions have small couplings to all KK’s (including graviton) based simply on the overlaps of the corresponding profiles, while the top quark and Higgs have a large coupling to the KK’s. To repeat, light SM fermions are localized near the Planck brane and photon, gluon and transverse W/Z have flat profiles, whereas all KK’s, Higgs (including longitudinal W/Z) and top quark are localized near the TeV brane. Schematically, neglecting effects related to electroweak symmetry breaking (EWSB), we find the following ratio of RS1 to SM gauge couplings:

$$\begin{aligned}
\frac{g_{\text{RS}}^{q\bar{q},l\bar{l}A^{(1)}}}{g_{\text{SM}}} &\simeq -\xi^{-1} \approx -\frac{1}{5} \\
\frac{g_{\text{RS}}^{Q^3\bar{Q}^3A^{(1)}}}{g_{\text{SM}}}, \frac{g_{\text{RS}}^{t_R\bar{t}_RA^{(1)}}}{g_{\text{SM}}} &\simeq 1 \text{ to } \xi (\approx 5) \\
\frac{g_{\text{RS}}^{HHA^{(1)}}}{g_{\text{SM}}} &\simeq \xi \approx 5 \quad (H = h, W_L, Z_L) \\
\frac{g_{\text{RS}}^{A^{(0)}A^{(0)}A^{(1)}}}{g_{\text{SM}}} &\sim 0
\end{aligned} \tag{1}$$

Here $q = u, d, s, c, b_R$, $l = \text{all leptons}$, $Q^3 = (t, b)_L$, and $A^{(0)}$ ($A^{(1)}$) correspond to zero (first KK) states of the gauge fields. Also, $g_{\text{RS}}^{xyz}, g_{\text{SM}}$ stands for the RS1 and the three SM (i.e., $4D$) gauge couplings respectively. Note that H includes both the physical Higgs (h) and *unphysical* Higgs, i.e., *longitudinal* W/Z by the equivalence theorem (the derivative involved in this coupling is similar for RS1 and SM cases and hence is not shown for simplicity). Finally, the parameter ξ is related to the Planck-weak hierarchy: $\xi \equiv \sqrt{k\pi r_c}$.

We also present the couplings of the KK graviton to the SM particles. These couplings involve derivatives (for the case of *all* SM particles), but (apart from a factor from the overlap

³Note that at the expense of giving up solving flavor hierarchy, it is possible to make the light generation up-type RH fermions localized towards the TeV brane with employing flavor symmetry, and, thereby, changing the production cross section and branching ratios of KK particles, which is also motivated by the possibility of improving naturalness [13].

of the profiles) it turns out that this energy-momentum dependence is compensated (or made dimensionless) by the $\bar{M}_P e^{-k\pi r_c} \sim \text{TeV}$ scale, instead of the \bar{M}_P -suppressed coupling to the SM graviton. Again, schematically:

$$\begin{aligned}
g_{\text{RS}}^{q\bar{q}, \ell\bar{\ell} G^{(1)}} &\sim \frac{E}{\bar{M}_P e^{-k\pi r_c}} \times 4D \text{ Yukawa} \\
g_{\text{RS}}^{A^{(0)} A^{(0)} G^{(1)}} &\sim \frac{1}{k\pi r_c} \frac{E^2}{\bar{M}_P e^{-k\pi r_c}} \\
g_{\text{RS}}^{Q^3 \bar{Q}^3 A^{(1)}}, g_{\text{RS}}^{t_R \bar{t}_R G^{(1)}} &\sim \left(\frac{1}{k\pi r_c} \text{ to } 1 \right) \frac{E}{\bar{M}_P e^{-k\pi r_c}} \\
g_{\text{RS}}^{HH G^{(1)}} &\sim \frac{E^2}{\bar{M}_P e^{-k\pi r_c}}
\end{aligned} \tag{2}$$

Here, $G^{(1)}$ is the KK graviton and the tensor structure of the couplings is not shown for simplicity.

2.3 Couplings of radion

In addition to the KK excitations of the SM, there is a particle, denoted by the “radion”, which is roughly the degree of freedom corresponding to the fluctuations of the size of extra dimension, and typically has a mass at the weak scale. It has Higgs-like properties: see [19] for details.

2.4 Masses

As indicated above, masses below about 2 TeV for gauge KK particles (note that these are the same for gluon, Z , W and denoted by M_{KK}) are strongly disfavored by precision tests, whereas masses for other KK particles are expected (in the general framework) to be of similar size to gauge KK mass and hence are (in turn) also constrained to be above 2 TeV. However, *direct* constraints on masses of other (than gauge) KK particles can be weaker. The radion mass can vary from ~ 100 GeV to ~ 2 TeV. In *minimal* models, KK graviton is actually about 1.5 heavier than gauge KK modes, i.e., at least 3 TeV.

As far as KK fermions are concerned, in minimal models, they have typically masses same as (or slightly heavier than) gauge KK and hence are constrained to be heavier than 2 TeV (in turn, based on masses of gauge KK required to satisfy precision tests). However, the masses of the KK excitations of top/bottom (and their other gauge-group partners) in some non-minimal (but well-motivated) models (where the $5D$ gauge symmetry is extended beyond that in the SM) can be (much) smaller than gauge KK modes, possibly even ~ 500 GeV.

3 Direct KK signals at the LHC, i.e., production

Based on the above KK couplings and masses, we are faced with the following challenges in obtaining signals at the LHC from direct production of the KK modes, namely,

- (i) Cross-section for production of these states is suppressed to begin with due to a small coupling to the protons’ constituents, and due to the large mass of the new particles;
- (ii) Decays to “golden” channels (leptons, photons) are suppressed. Instead, the decays are dominated by top quark and Higgs (including longitudinal W/Z);
- (iii) These resonances tend to be quite broad due to the enhanced couplings to top quark/Higgs.

- (iv) The SM particles, namely, top quarks/Higgs/ W/Z gauge bosons, produced in the decays of the heavy KK particles are highly boosted, resulting in a high degree of collimation of the SM particles' decay products. Hence, conventional methods for identifying top quark/Higgs/ W/Z might no longer work for such a situation.

However, such challenges also present research opportunities, for example, techniques for identification of boosted top quark/Higgs/ W/Z have been developed [20].

The following table summarizes the production cross-sections for the spin-1 and spin-2 KK particles at the 14 TeV LHC (with KK mass set to 3 TeV) and the dominant decay channels. Based on the above discussion, note that the polarization of W/Z 's in these decay channels is dominantly *longitudinal*. The bottom quark is LH, but the top quark can be either LH or RH. Some more details are in the sections that follow.

KK particle	total σ (fb)	(SM) final states	references
graviton	~ 0.1 for $k \sim M_{\text{Pl}}$	$t\bar{t}, b\bar{b}, WW, hh, ZZ$	hep-ph/0701186
gluon	~ 100	$t\bar{t}, b\bar{b}$	0706.3960
Z	a few	$t\bar{t}, b\bar{b}, Zh, WW$	0709.0007
W	10	$WZ, Wh, t\bar{b}$	0810.1497

In the following sections, we give details of studies of the KK particles in this framework performed as part of the Snowmass 2013 process: for more details of the specific models (including previous studies), see corresponding references given in each title and for an overview, see reference [21].

3.1 A proposal for Two “Benchmarks” [22]

In order to begin this discussion, we mention the benchmark models studied. The color $[SU(3)_c]$ structure is standard and is thus not shown. On the other hand, the electroweak (EW) gauge group is extended: $SU(2)_L \times SU(2)_R \times U(1)_X$ (as motivated by relaxing the constraint from the T parameter). The extra gauge bosons (relative to the SM) can be taken (by a suitable choice of boundary conditions) to have no zero-modes. The hypercharge is then given by $Y = T_{3R} + X$.

In the light of the large top mass, depending on 5D Yukawa coupling, it is clear that either (or both) LH and RH top have to be localized near the TeV brane. However if it is the LH top, then so is LH bottom thus creating a constraint from shift in $Zb\bar{b}$ coupling. On the other hand, the coupling to Z of t_R as not been precisely measured thus far and hence such a localization of t_R poses less of a constraint.

In order to alleviate the above constraint, i.e., have the custodial symmetry protection of the $Zb\bar{b}$ coupling [17], we take the third generation left-handed quarks to be in the representation⁴

$$Q_L^3 = (q_L^3 \quad q_L'^3) = \begin{pmatrix} t_L & \chi_L \\ b_L & T_L \end{pmatrix} \rightarrow (2, 2)_{2/3} \text{ (for both cases I and II: see below) ,} \quad (3)$$

where χ_L, T_L are taken to have no zero-modes⁵. We have $Q(\chi_L) = 5/3$ and $Q(T_L) = 2/3$. To accommodate the large top and bottom mass difference we take it that t_R and b_R do not belong

⁴In addition, the two 5D $SU(2)$ gauge couplings are taken to be equal. The “canonical” choice would be that LH fermions are singlets of $SU(2)_R$.

⁵Only the 5D fermions with SM quantum numbers can have zero modes.

to the same $SU(2)_R$ multiplet. With the above choice, one can contemplate Q_L^3 being localized near the TeV brane.

We consider two cases for the t_R representations

$$\begin{aligned} \text{Case I} & : \quad t_R \rightarrow (1, 3)_{2/3} \oplus (3, 1)_{2/3} = \begin{pmatrix} \chi_R'' \\ t_R \\ B_R'' \end{pmatrix} \oplus \begin{pmatrix} \chi_R''' \\ T_R''' \\ B_R''' \end{pmatrix} , \\ \text{Case II} & : \quad t_R \rightarrow (1, 1)_{2/3} , \end{aligned} \tag{4}$$

where (once again) the extra fermions are chosen to have no zero-modes.

For Case II, $t_R \rightarrow (1, 1)$, the electroweak precision tests (EWPT) are better satisfied for Q_L^3 peaked closer to the TeV brane, while for Case I, $t_R \rightarrow (1, 3)$, for t_R peaked closer to the TeV brane. So, we choose

$$\begin{aligned} \text{Case I} & : \quad c_{Q_L^3} = 0.4 \text{ and } c_{t_R} = 0 , \\ \text{Case II} & : \quad c_{Q_L^3} = 0 \text{ and } c_{t_R} = 0.4 \end{aligned} \tag{5}$$

After including the charges and the overlap integrals, the largest effective coupling of third generation fermions to gauge KK modes in Case II would be to Q_L^3 , being larger than that in Case I, which would be to t_R . Consequently, in Case I, the bottom quark is essentially not in the game, where it is in Case II. Thus, while on the one hand new gauge KK induced FCNC contributions would be larger in Case II (again since b_L and hence down sector flavor violation is involved) and hence more problematic for the simplest constructions, on the other hand collider signals would be larger compared to Case I (for example, KK W decays to $t\bar{b}$ would be suppressed in case I, but significant in case II).

Also, the polarization of top quark resulting from the production and decay of KK particles is different in the two cases and hence this measurement can distinguish them.

Finally, note that

- exact localization of other (light) fermions is basically irrelevant for LHC signals (as long as they are localized near the Planck brane, i.e., $c \gtrsim 1/2$, as we assume here). Hence the values of c 's for them are not explicitly shown.

3.2 Sensitivity to narrow $t\bar{t}$ resonances in the all-hadronic decay channel

As seen from table 3, most spin-1 and spin-2 KK particles in the warped extra dimensional framework have significant BR to decay into $t\bar{t}$. Also, in other models, there are Z' which are leptophobic and thus have to be searched for via decays into quarks, in particular, top. So, it is very useful to perform a general study of $t\bar{t}$ resonances, which is the goal of this section.

In order to predict the expected sensitivity to narrow $t\bar{t}$ resonances at the 14 TeV LHC, we perform a search in the all-hadronic decay channel. The expected cross section limits are quoted for resonance masses of 2, 3, 4 and 5 TeV assuming 300 fb^{-1} and 3000 fb^{-1} of integrated luminosity. Those systematic effects which are expected to dominate are taken into account. The cross section limits are interpreted as limits on the mass of a leptophobic top-color Z' boson [23] in this section, as well as limits on the masses of KK gravitons and KK Z' bosons in Sec. 3.3 and 3.5, respectively⁶.

⁶KK gluon in the warped extra dimensional framework tends to be rather broad so that it might not be possible to directly translate the results of this study into bounds on KK gluon.

Z' signal samples are generated using Pythia [24] with a narrow resonance width. The background processes, Standard Model $t\bar{t}$ production and QCD multijet production, are generated with Herwig++ [25], with a minimum p_T requirement of 650 GeV on the two highest- p_T partons required at generator level. All samples are overlaid with simulated minimum-bias events corresponding to three pile-up scenarios with an average number of interactions per bunch-crossing of $\mu = 0, 50$ and 140. The samples are then reconstructed using version 3.0.9 of the DELPHES fast detector simulation [26] using the Snowmass detector [27].

While the background cross sections are obtained at LO from the Herwig++ generator, the signal cross sections for Z' production calculated in Ref. [28] for a resonance width of 1.2% are used, and a k -factor of 1.3 is applied [29]. Tab. 1 shows an overview of the cross sections considered at leading order (LO).

Table 1: LO cross sections considered in the analysis in the $t\bar{t}$ all-hadronic final state.

sample	cross section
Z' (2 TeV)	214 fb
Z' (3 TeV)	23.2 fb
Z' (4 TeV)	3.24 fb
Z' (5 TeV)	0.553 fb
$t\bar{t}$ ($p_T > 650$ GeV)	$1.28 \cdot 10^3$ fb
QCD multijet ($p_T > 650$ GeV)	$170 \cdot 10^3$ fb

Large- R jets are reconstructed with the Cambridge-Aachen [30] algorithm with a radius parameter of 0.8. They must fulfill $p_T > 750$ GeV and $|\eta| < 2.0$. Top-tagging is implemented requiring the trimmed jet mass, m , to be larger than 80 GeV, and the largest di-subjet mass when the jet is de-clustered to three subjets, Q_W , to be larger than 70 GeV. This top-tagging criterion was optimized using the ratio of the tagging efficiency for top quarks over the square root of the mis-tagging efficiency for non-top jets. A variety of substructure variables was taken into account, such as k_t splitting scales, N -subjettiness variables and the number of subjets. Adding more variables to the top quark identification does not help to increase the performance significantly.

The decreasing b -tagging efficiency, ε , and b -tagging rejection of light quark jets, r , at high jet p_T is taken into account by applying b -tagging weights to jets instead of using the default b -tagging as implemented in the Snowmass detector:

$$\varepsilon(p_T) = 0.83 \cdot \exp(-0.68 \cdot p_T[\text{TeV}]) \quad , \quad r(p_T) = 80 \cdot \exp(-0.92 \cdot p_T[\text{TeV}]) \quad .$$

Benchmarks of $\varepsilon(750 \text{ GeV}) \approx 50\%$, $\varepsilon(1500 \text{ GeV}) \approx 30\%$, $r(750 \text{ GeV}) \approx 40$ and $r(1500 \text{ GeV}) \approx 20$ were used to parametrize the curves. In order to take into account the degradation of b -tagging algorithms with increasing pile-up, the fake rate, $f = \frac{1}{r}$, is increased by $\frac{1}{3}$ ($\frac{2}{3}$) for $\mu = 50$ (140).

In order to select events for the analysis, two top- and b -tagged large- R jets with $p_T > 750$ GeV are required and the di-jet invariant mass is calculated. A signal window of ± 500 GeV is chosen around the resonance mass for the statistical analysis, as shown for one example in Fig. 1.

Four sources of systematic uncertainties are considered:

- An overall normalization uncertainty of the Standard Model $t\bar{t}$ background of 10% is assumed. With data, it may be constraint by the use of a $t\bar{t}$ dominated control region.

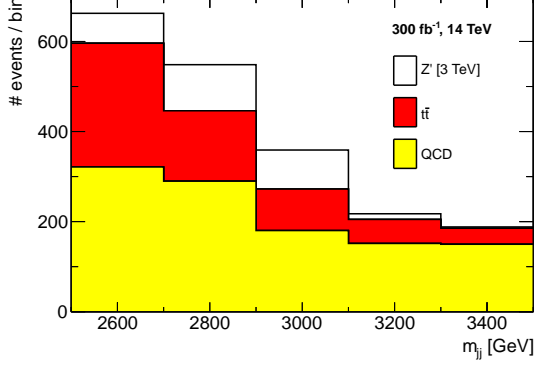


Figure 1: Reconstructed Z' mass distribution in the all-hadronic channel for a resonance mass of 3 TeV, 300 fb^{-1} of 14 TeV data and $\mu = 50$. The signal distribution is shown on top of the background contributions.

- An overall normalization uncertainty of the QCD multijet background of 50% is assumed, which reflects the extrapolation uncertainty of the data-driven estimate of the QCD multijet background from a control region into the signal region.
- The jet energy uncertainty is assumed to be 2% of the jet p_T . It is evaluated for signal and the Standard Model $t\bar{t}$ background, because the QCD multijet background is assumed to be estimated in a data-driven way.
- The uncertainty on the b -tagging efficiency is assumed to be 10% and is, analogously to the jet energy uncertainty, evaluated for signal and $t\bar{t}$ background.

All sources of systematic uncertainties are only considered as a change of the yield of the corresponding process. The effects on the shape of the invariant di-jet mass spectrum are neglected.

The Bayesian Analysis Toolkit [31] is used to determine the 95% CL upper limits on the signal cross section for each mass point given the SM mass spectrum and that of a given signal model. Systematic uncertainties are taken into account as nuisance parameters of the fit, hence strongly constraining the mostly unconstrained QCD multijet background with its prior normalization uncertainty of 50%.

Fig. 2 shows the expected cross section exclusion as a function of the Z' mass for 300 fb^{-1} of 14 TeV data and $\mu = 50$ (left), and for 3000 fb^{-1} of data and $\mu = 140$ (right). The mass reach for both scenarios is 3.7 and 4.1 TeV, respectively. Tab. 2 gives an overview of the cross section limits for the different resonance masses and pile-up scenarios, as well as for the two different integrated luminosities.

In summary, it can be stated that with 300 fb^{-1} of data at 14 TeV, leptophobic top-color Z' bosons with the above parameters can be excluded up to masses of 3.7 TeV using this analysis in the all-hadronic $t\bar{t}$ decay channel. With ten times more data, taking into account the more challenging pile-up conditions, the mass reach is increased to 4.1 TeV.

3.3 KK graviton [32]

Armed with the above benchmarks models, we now discuss searches for each type of KK particle in turn. The dominant production is via gluon fusion and decay channels for KK graviton are

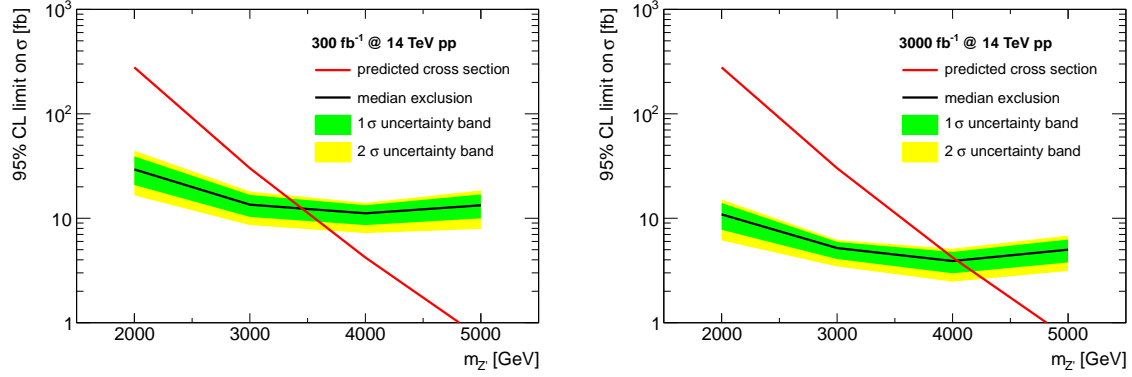


Figure 2: Expected cross section upper limits at 95% CL for a leptophobic top-color Z' boson with a width of 1.2% decaying to a top quark pair in the all-hadronic channel. The left plot shows the limits for 300 fb^{-1} of 14 TeV data and $\mu = 50$. The right plot shows the limits for 3000 fb^{-1} of data and $\mu = 140$ (right). The mass reach is 3.7 (4.1) TeV for 300 (3000) fb^{-1} .

Table 2: 95% CL limits for a leptophobic top-color Z' boson with a width of 1.2% decaying to a top quark pair in the all-hadronic channel. Limits are given for different resonance masses, pile-up scenarios and integrated luminosities. The expected mass exclusion is also shown.

lumi.	pile-up	uncertainties	$m = 2 \text{ TeV}$	3 TeV	4 TeV	5 TeV	mass reach
300 fb^{-1}	$\mu = 0$	stat.	16 fb	6.4 fb	5.3 fb	6.6 fb	4.0 TeV
300 fb^{-1}	$\mu = 0$	stat.+syst.	26 fb	12 fb	10 fb	11 fb	3.8 TeV
300 fb^{-1}	$\mu = 50$	stat.	16 fb	6.7 fb	5.7 fb	7.6 fb	3.9 TeV
300 fb^{-1}	$\mu = 50$	stat.+syst.	29 fb	13 fb	11 fb	13 fb	3.7 TeV
300 fb^{-1}	$\mu = 140$	stat.	17 fb	7.2 fb	6.2 fb	8.5 fb	3.9 TeV
300 fb^{-1}	$\mu = 140$	stat.+syst.	35 fb	15 fb	12 fb	15 fb	3.7 TeV
3000 fb^{-1}	$\mu = 0$	stat.	4.9 fb	2.0 fb	1.5 fb	1.9 fb	4.7 TeV
3000 fb^{-1}	$\mu = 0$	stat.+syst.	8.1 fb	3.6 fb	3.3 fb	3.3 fb	4.3 TeV
3000 fb^{-1}	$\mu = 50$	stat.	5.0 fb	2.1 fb	1.7 fb	2.2 fb	4.6 TeV
3000 fb^{-1}	$\mu = 50$	stat.+syst.	8.7 fb	4.3 fb	3.6 fb	4.3 fb	4.1 TeV
3000 fb^{-1}	$\mu = 140$	stat.	5.4 fb	2.2 fb	1.9 fb	2.5 fb	4.6 TeV
3000 fb^{-1}	$\mu = 140$	stat.+syst.	11 fb	5.2 fb	3.9 fb	5.0 fb	4.1 TeV

into $t\bar{t}$, WW , ZZ , hh :

$$gg \rightarrow \text{KK graviton} \rightarrow ZZ, WW, hh \text{ (and } t\bar{t}, b\bar{b}) \quad (6)$$

For a 2 TeV KK graviton, each of these cross-sections can be $\sim O(10)$ fb with a total decay width of $\sim O(100)$ GeV.

In more detail, the production is governed by

$$\mathcal{L}_{\text{prod.}} = 0.053 \frac{c}{M_{G(1)}} \eta^{\mu\alpha} \eta^{\nu\beta} h_{\alpha\beta}^{(1)}(x) T_{\mu\nu}^{\text{gluon}}(x)$$

where $c = k/M_{\text{Pl}}$, $M_{G(1)}$ is KK graviton mass⁷ and $T_{\mu\nu}^{\text{gluon}}$ is 4D energy-momentum tensor of SM gluon⁸.

⁷As mentioned earlier, this mass is $\approx 1.5 M_{\text{KK}}$, where M_{KK} is the *gauge* KK mass.

⁸we set $\sqrt{k\pi r_c} = 5.83$ here

And, decay proceeds via

$$\mathcal{L}_{\text{decay}} \ni 3.83 \frac{c}{M_{G^{(1)}}} \eta^{\mu\alpha} \eta^{\nu\beta} h_{\alpha\beta}^{(1)}(x) T_{\mu\nu}^{t,b,H}(x)$$

This gives the total decay width:

	Case I	Case II
$\Gamma_{G^{(1)}}$	$0.063 \, c^2 M_{G^{(1)}}$	$0.107 \, c^2 M_{G^{(1)}}$

and the branching ratios (BRs):

	Case I	Case II
$(t, b)_L$	~ 0	9/22 each
t_R	9/13	~ 0
h	1/13	1/22
W_L	2/13	2/22
Z_L	1/13	1/22

After the above overview of KK graviton couplings, we discuss studies of two specific decay channels.

3.3.1 KK graviton $\rightarrow ZZ$

We estimate the KK graviton discovery potential at the LHC using the ZZ decay channel where one Z bosons decays leptonically and the other hadronically. For high graviton masses, the produced Z bosons are highly boosted and the two quarks from the hadronically decaying Z boson are expected to be inside the same jet. Thus the final state topology consists of two isolated leptons and one highly energetic massive jet. The events are selected using the following criteria:

$$p_{\perp}^l > 25 \text{ GeV} \quad p_{\perp}^j > 25 \text{ GeV}, \quad |\eta^{j,l}| < 2.4, \quad 66 \text{ GeV} < m_{ll} < 116 \text{ GeV}. \quad (7)$$

To reduce the background, the signal region is defined by requiring:

$$p_{\perp}^{ll} > 400 \text{ GeV}, \quad p_{\perp}^j > 400 \text{ GeV}, \quad m_j > 40 \text{ GeV} \quad (8)$$

The Z +Jets events form the dominant SM background. The background and the signal are both simulated with **MadGraph 5**. The model is implemented into **Madgraph 5** [33] using the **FeynRules** [34] package. The events are then passed to **Pythia 6** [35] for showering and hadronization. The **Delphes 3** program is used for fast detector simulation and for object reconstruction. The jets are reconstructed using the anti- k_t algorithm [36] with a radius parameter 0.6.

In Figs.3.a and 3.b we present the 95% confidence level exclusion plots for KK graviton mass in the decay channel $pp \rightarrow \text{KK graviton} \rightarrow ZZ \rightarrow \mu^+ \mu^- jj$ at the $\sqrt{s} = 14 \text{ TeV}$ and $\sqrt{s} = 33 \text{ TeV}$ respectively. On both plots, the blue dashed curve corresponds to the Case I (the t_R near TeV brane) while the solid green curve to the Case II (Q_L^3 near the TeV brane). The limits on the signal rate are determined using the CL_s method [37, 38].

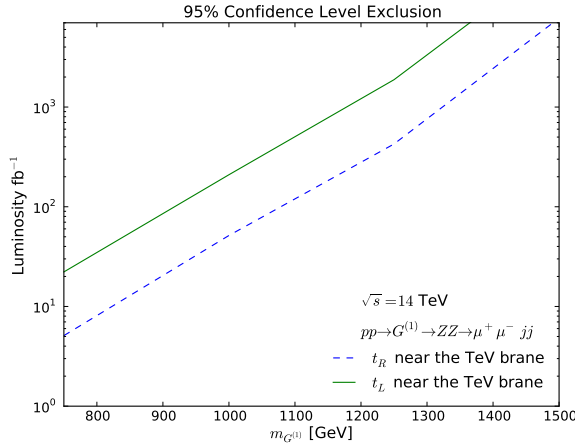


Figure 3.a The 95% confidence level exclusion for the KK graviton mass at $\sqrt{s} = 14$ TeV in the decay channel $pp \rightarrow G^{(1)} \rightarrow ZZ \rightarrow \mu^+ \mu^- jj$.

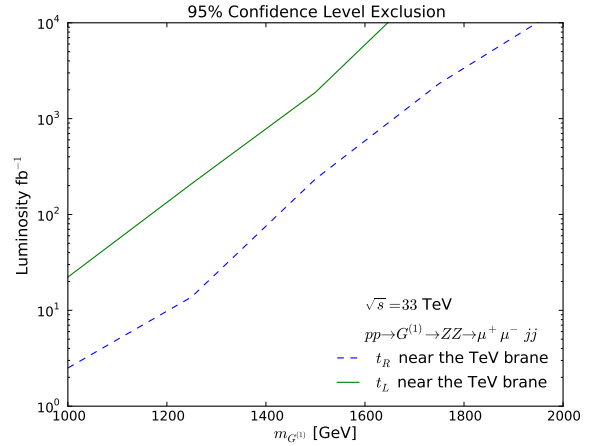


Figure 3.b The 95% confidence level exclusion for the KK graviton mass at $\sqrt{s} = 33$ TeV in the decay channel $pp \rightarrow G^{(1)} \rightarrow ZZ \rightarrow \mu^+ \mu^- jj$.

3.3.2 Reinterpretation of the search for narrow $t\bar{t}$ resonances

The search for narrow $t\bar{t}$ resonances in the all-hadronic final state described in Sec. 3.2 is reinterpreted in terms of limits on KK gravitons as discussed in Ref. [32] decaying to $t\bar{t}$. Four scenarios are investigated following the notation convention as in the reference:

- t_R near the TeV brane with $c = 0.5$,
- t_R near the TeV brane with $c = 1.0$,
- t_L near the TeV brane with $c = 0.5$, and
- t_L near the TeV brane with $c = 1.0$.

Tab. 3 shows the signal cross sections used in the reinterpretation. The k -factor of 1.3 used in the leptophobic top-color Z' analysis is also used here, although it has only limited validity in this scenario.

Figs. 4 and 5 show the 95% CL limits on the cross section of a narrow resonance overlaid with the expected cross sections for the KK graviton models. The mass limits for the KK gravitons are given in Tab. 4 for the different pile-up and luminosity scenarios for statistical uncertainties only and with systematic uncertainties included. If the mass limits is denoted < 2 TeV, the analysis is not sensitive to resonance mass above 2 TeV. With 3000 fb^{-1} of data at 14 TeV, KK gravitons can be excluded with masses up to 2.8 (2.3) TeV in the t_R (t_L) scenarios with $c = 1.0$. For $c = 0.5$, however, the sensitivity does not reach 2 TeV for the resonance mass when systematic uncertainties are taken into account.

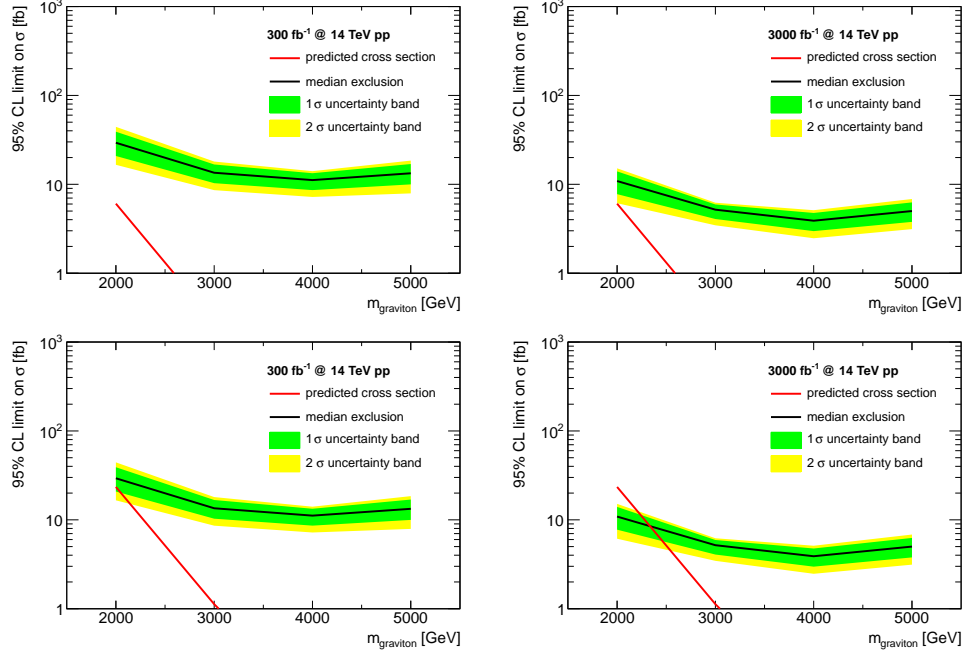


Figure 4: Expected cross section upper limits at 95% CL for the t_R KK graviton model with parameter $c = 0.5$ and $c = 1.0$ (upper and lower plots) decaying to a top quark pair in the all-hadronic channel. The left plots show the limits for 300 fb^{-1} of 14 TeV data and $\mu = 50$. The right plots show the limits for 3000 fb^{-1} of data and $\mu = 140$ (right).

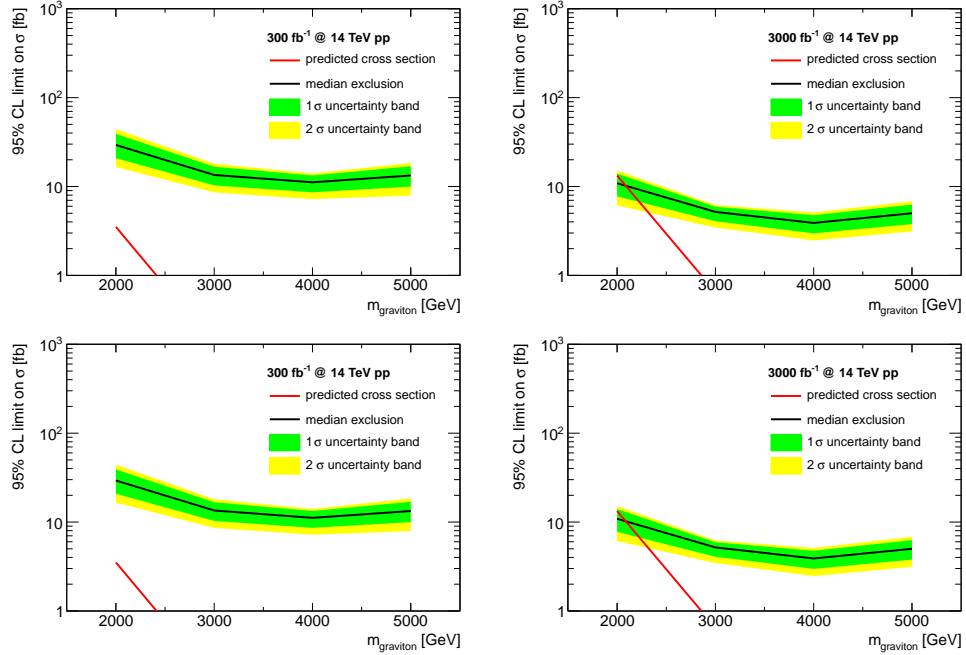


Figure 5: Expected cross section upper limits at 95% CL for the t_L KK graviton model with parameter $c = 0.5$ and $c = 1.0$ (upper and lower plots) decaying to a top quark pair in the all-hadronic channel. The left plots show the limits for 300 fb^{-1} of 14 TeV data and $\mu = 50$. The right plots show the limits for 3000 fb^{-1} of data and $\mu = 140$ (right).

Table 3: Cross sections at 14 TeV considered in the analysis of the search for narrow $t\bar{t}$ resonances.

scenario	KK graviton mass	cross section
R 0.5	2 TeV	4.7 fb
R 0.5	3 TeV	0.22 fb
R 0.5	4 TeV	0.016 fb
R 0.5	5 TeV	0.0014 fb
R 1.0	2 TeV	18 fb
R 1.0	3 TeV	0.87 fb
R 1.0	4 TeV	0.066 fb
R 1.0	5 TeV	0.0065 fb
L 0.5	2 TeV	2.7 fb
L 0.5	3 TeV	0.13 fb
L 0.5	4 TeV	0.0096 fb
L 0.5	5 TeV	0.00088 fb
L 1.0	2 TeV	10 fb
L 1.0	3 TeV	0.50 fb
L 1.0	4 TeV	0.040 fb
L 1.0	5 TeV	0.0042 fb

3.4 KK gluon [39]

Kinematics of heavy s -channel resonance decays are characterized by decay products with a significant boost. The energy frontier searches for heavy di-top resonances thus hinge on our ability to efficiently tag highly energetic top quarks. Identifying boosted tops with $p_T < 1$ TeV has become possible in the light of numerous recent developments in the field of jet substructure [40, 41, 42, 43, 44, 45, 46, 47, 48], while efficiently tagging the tops in the ultra-high boosted regime (e.g. $p_T > 1$ TeV) remains a challenge. In this section, using RS KK gluon as an example, we estimate the discovery potential for a top pair resonance in the future 14 TeV LHC experiment using jet substructure techniques (more precisely, the Template Overlap Method (TOM) [47]). TOM has been extensively studied in the past in the context of theoretical studies of boosted top and boosted Higgs decays [44, 47, 49], as well as used by the ATLAS collaboration for a boosted resonance search [50] at $\sqrt{s} = 7$ TeV. The method is designed to match the energy distribution of a boosted jet to the parton-level configuration of a boosted top decay, with all kinematic constraints taken into account. Because our analysis focuses on events in which one top decays hadronically and the other semi-leptonically, we employ two different formulations of TOM. The hadronic TOM which is designed to tag the fully hadronic decays of the top, and the leptonic TOM [51], designed to take into account decays with missing energy⁹. The latter is particularly useful in compensating for the loss of rejection power due to the absence of efficient b -tagging methods at high p_T .

Low susceptibility to intermediate levels of pileup (i.e. 20-50 interactions per bunch crossing), makes TOM particularly attractive for boosted top analyses at the LHC. Refs. [49, 51] showed that the ability of TOM to tag the top jets is nearly unaffected even at 20-50 interactions per bunch crossing, with the W +jets mistag rate changing by as little as 10% at, thus nearly eliminating the need for pileup subtraction / correction at intermediate pileup levels.

⁹We use the TemplateTagger v.2.0 [52] implementation of TOM for both the hadronic and the leptonic formulations.

Table 4: 95% CL limits on the resonance mass for the two KK graviton models with $c = 0.5$ and $c = 1.0$ decaying to a top quark pair in the all-hadronic channel. Limits are given for pile-up scenarios and integrated luminosities.

scenario	lumi.	pile-up	uncertainties	mass reach
R 0.5	300 fb ⁻¹	$\mu = 0$	stat.	< 2 TeV
R 0.5	300 fb ⁻¹	$\mu = 0$	stat.+syst.	< 2 TeV
R 0.5	300 fb ⁻¹	$\mu = 50$	stat.	< 2 TeV
R 0.5	300 fb ⁻¹	$\mu = 50$	stat.+syst.	< 2 TeV
R 0.5	300 fb ⁻¹	$\mu = 140$	stat.	< 2 TeV
R 0.5	300 fb ⁻¹	$\mu = 140$	stat.+syst.	< 2 TeV
R 0.5	3000 fb ⁻¹	$\mu = 0$	stat.	2.4 TeV
R 0.5	3000 fb ⁻¹	$\mu = 0$	stat.+syst.	< 2 TeV
R 0.5	3000 fb ⁻¹	$\mu = 50$	stat.	2.3 TeV
R 0.5	3000 fb ⁻¹	$\mu = 50$	stat.+syst.	< 2 TeV
R 0.5	3000 fb ⁻¹	$\mu = 140$	stat.	2.3 TeV
R 0.5	3000 fb ⁻¹	$\mu = 140$	stat.+syst.	< 2 TeV
R 1.0	300 fb ⁻¹	$\mu = 0$	stat.	2.6 TeV
R 1.0	300 fb ⁻¹	$\mu = 0$	stat.+syst.	< 2 TeV
R 1.0	300 fb ⁻¹	$\mu = 50$	stat.	2.6 TeV
R 1.0	300 fb ⁻¹	$\mu = 50$	stat.+syst.	< 2 TeV
R 1.0	300 fb ⁻¹	$\mu = 140$	stat.	2.5 TeV
R 1.0	300 fb ⁻¹	$\mu = 140$	stat.+syst.	< 2 TeV
R 1.0	3000 fb ⁻¹	$\mu = 0$	stat.	3.0 TeV
R 1.0	3000 fb ⁻¹	$\mu = 0$	stat.+syst.	2.9 TeV
R 1.0	3000 fb ⁻¹	$\mu = 50$	stat.	2.9 TeV
R 1.0	3000 fb ⁻¹	$\mu = 50$	stat.+syst.	2.8 TeV
R 1.0	3000 fb ⁻¹	$\mu = 140$	stat.	2.9 TeV
R 1.0	3000 fb ⁻¹	$\mu = 140$	stat.+syst.	2.8 TeV
L 0.5	300 fb ⁻¹	$\mu = 0$	stat.	< 2 TeV
L 0.5	300 fb ⁻¹	$\mu = 0$	stat.+syst.	< 2 TeV
L 0.5	300 fb ⁻¹	$\mu = 50$	stat.	< 2 TeV
L 0.5	300 fb ⁻¹	$\mu = 50$	stat.+syst.	< 2 TeV
L 0.5	300 fb ⁻¹	$\mu = 140$	stat.	< 2 TeV
L 0.5	300 fb ⁻¹	$\mu = 140$	stat.+syst.	< 2 TeV
L 0.5	3000 fb ⁻¹	$\mu = 0$	stat.	< 2 TeV
L 0.5	3000 fb ⁻¹	$\mu = 0$	stat.+syst.	< 2 TeV
L 0.5	3000 fb ⁻¹	$\mu = 50$	stat.	< 2 TeV
L 0.5	3000 fb ⁻¹	$\mu = 50$	stat.+syst.	< 2 TeV
L 0.5	3000 fb ⁻¹	$\mu = 140$	stat.	< 2 TeV
L 0.5	3000 fb ⁻¹	$\mu = 140$	stat.+syst.	< 2 TeV
L 1.0	300 fb ⁻¹	$\mu = 0$	stat.	< 2 TeV
L 1.0	300 fb ⁻¹	$\mu = 0$	stat.+syst.	< 2 TeV
L 1.0	300 fb ⁻¹	$\mu = 50$	stat.	< 2 TeV
L 1.0	300 fb ⁻¹	$\mu = 50$	stat.+syst.	< 2 TeV
L 1.0	300 fb ⁻¹	$\mu = 140$	stat.	< 2 TeV
L 1.0	300 fb ⁻¹	$\mu = 140$	stat.+syst.	< 2 TeV
L 1.0	3000 fb ⁻¹	$\mu = 0$	stat.	2.9 TeV
L 1.0	3000 fb ⁻¹	$\mu = 0$	stat.+syst.	2.6 TeV
L 1.0	3000 fb ⁻¹	$\mu = 50$	stat.	2.9 TeV
L 1.0	3000 fb ⁻¹	$\mu = 50$	stat.+syst.	2.6 TeV
L 1.0	3000 fb ⁻¹	$\mu = 140$	stat.	2.8 TeV
L 1.0	3000 fb ⁻¹	$\mu = 140$	stat.+syst.	2.3 TeV

3.4.1 Template Overlap Method

We begin with the definition of the hadronic peak template overlap [44, 47, 49]:

$$Ov_3^h(j, f[j]) = \max_{\{f\}} \left[\exp \left[- \sum_{a=1}^3 \frac{1}{\sigma_a^2} \left(\epsilon p_{T,a} - \sum_{i \in j} p_{T,i} F(\hat{n}_i, \hat{n}_a) \right)^2 \right] \right], \quad (9)$$

where $p_{T,a}$ is the transverse momentum of the a^{th} template parton, $p_{T,i}$ is the transverse momentum of the i^{th} jet constituent and f is the set of all possible parton level configurations which satisfy the kinematic constraints of a boosted top decay (called “templates”):

$$\sum_a p_{T,a} = P, \quad P^2 = m_t^2, \quad (p_1 + p_2)^2 = m_W^2, \quad (10)$$

where $p_{1,2}$ are two of the three template momenta and P is the four momentum of the boosted top.

The function $F(\hat{n}_i, \hat{n}_a)$ restricts the sum over i and a to non-intersecting angular regions centered around each template momentum p_a :

$$F(\hat{n}_i, \hat{n}_a) = \begin{cases} 1 & \text{if } \Delta R < r_a \\ 0 & \text{otherwise} \end{cases}, \quad (11)$$

where $\Delta R = \sqrt{\delta\phi^2 + \delta\eta^2}$ is the distance between the template parton and the jet constituent.

The coefficient ϵ in Eq. 9 compensates for the energy deposited outside the template sub-cone, while the weight σ_a defines the resolution of the observable Ov_3^h . Here we use $\sigma_a = p_{T,a}/3$. For simplicity, we will keep all $\epsilon = 1$, without the loss of generality or significant effects on the mass reach of resonance searches.

Similar to Eq. 9 we use the definition of leptonic peak overlap of Ref. [51]:

$$Ov_3^l = \max_{\{f\}} \left[\underbrace{\exp \frac{-1}{\sigma_b^2} \left(\epsilon k_{T,b} - \sum_{i \in j} p_{T,i} F(\hat{n}_i, \hat{n}_a) \right)^2}_{\text{b quark}} \underbrace{\exp \frac{-1}{\sigma_l^2} (\epsilon_l k_{T,l} - p_{T,l})^2}_{\text{lepton}} \underbrace{\exp \frac{-1}{\sigma_\nu^2} (\epsilon_\nu k_{T,\nu} - \cancel{E}_T F'(\phi_\nu, \phi_{\cancel{E}_T}))^2}_{\text{neutrino}} \right], \quad (12)$$

where F' is defined as

$$F'(\phi_\nu, \phi_{\cancel{E}_T}) = \begin{cases} 1 & \text{if } \Delta\phi_{\nu, \cancel{E}_T} < r_\nu \\ 0 & \text{otherwise} \end{cases}, \quad (13)$$

and $\Delta\phi$ is the azimuthal distance between the template parton and the total \cancel{E}_T .

The Ov_3^l definition differs from Eq. 9 in two major ways. First, Eq. 12 explicitly keeps track of the particle species and second, only the transverse component of the missing energy is taken into account. We choose to rotate each leptonic top template into the frame in which the first template parton is aligned with the lepton, due to the absence of a well defined “jet axis”. Note that the two formulations of template overlap are compatible enough so that the same set of template states can be used in both.

For the purpose of our analysis, we generate the template sets in the boosted top frame at fixed transverse momentum with a sequential scan in 50 steps in η, ϕ for the first two template momenta, while the third parton is determined by conservation of energy. We consider a range of $p_T = 500 - 1600$ GeV in steps of 100 GeV, resulting in 12 template p_T bins.

For hadronic top templates we use fixed template sub-cones at fixed template p_T , with dependence of the sub-cone size with the transverse momentum of the boosted top described by the scaling rule

$$r_a(p_{T,a}) = \frac{70 \text{ GeV}}{p_{T,a}}, \quad (14)$$

where we limit the range of r_a to the interval of $[0.07, 0.3]$. The lower limit on the template sub cone size serves to take into account the detector resolution, as well as match the optimal value for the template sub cone at $p_T = 1 \text{ TeV}$.

The leptonic top template for the b quark uses the same scaling rule of Eq. 14, while for the neutrino we use a fixed $r_\nu = 0.2$.

The output of TOM is not limited to the peak overlap score, $OV_3^{h,l}$. Additional information about the boosted top decay is contained in the peak template momenta. An additional correlation, useful in discriminating boosted tops from light jets is Template Planar Flow [47]:

$$tPf \equiv \frac{4 \det(I)}{\text{tr}(I)^2}, \quad (15)$$

where

$$I^{kl} \equiv \frac{1}{m_t} \sum_{i=1}^3 \frac{p_k^i p_l^i}{p_T^i},$$

and $p_k^i \equiv p_T^i(\eta^i, \phi^i)$ are the two-vectors constructed from p_T, η, ϕ of the three peak template momenta. Template planar flow is useful in distinguishing decay configurations which lie on a straight line in the plane perpendicular to the top boost (low $tPf \approx 0$) from the decays which are not aligned on a line ($tPf \approx 1$). The formulation of tPf is similar to Jet Planar Flow, with an important difference that it is intrinsically infra-red safe and weakly sensitive to pileup.

3.4.2 Results

We consider two Snowmass benchmark points: the Case 1 RS KK gluon (Right handed, top near the brane) of $M_{G'_{KK}} = 3, 5 \text{ TeV}$, and a Case 2 RS KK gluon (Left handed, bottom near the brane) with $M_{G'_{KK}} = 3, 5 \text{ TeV}$ as well. The coupling strengths to left and right heavy quarks in both cases are given in Table 5, while for production, we take the coupling to light quarks to be -0.2 of SM QCD (for both Cases 1 and 2). Note that the SM QCD coupling here should be evaluated at a few TeV.

We consider a signal of the form

$$q\bar{q} \rightarrow \text{KK gluon} \rightarrow t\bar{t}, \quad (16)$$

where we require one top to decay hadronically and the other leptonically. The main background channels consist of SM $t\bar{t}$ and Wjj .

We generate the data using MadGraph [33] + Pythia [24], with CTEQ6M [53] parton distribution functions at $\sqrt{s} = 14 \text{ TeV}$, while jet clustering is performed using the FastJet [54] implementation of the anti- k_T algorithm with a jet cone of $R = 1.0$ for the fat jet. All SM events are matched to an extra jet using the MLM matching [55] prescription. Note that we do not impose an implicit mass window on the top jets, and instead rely on the intrinsic mass filtering ability of TOM as a pileup insensitive alternative to a mass window.

We separately analyze events with no pileup and with $\langle N_{vtx} \rangle = 50$ interactions per bunch crossing in order to illustrate the effects of pileup on the analysis. Note that we do not employ any

	Case 1	Case 2
$(t, b)_L$	1	3.9
t_R	3.9	1

Table 5: Coupling strengths of the KK gluon to the left/right heavy flavors for the Case 1 and 2 benchmark points.

pileup subtraction / correction to the events, but instead focus on observables which are weakly sensitive to pileup. For instance, we determine the transverse momentum of the hadronically decaying top based on the scalar sum of the transverse momenta of the decay products of the leptonic top which recoils against it. The method serves both as a pileup-insensitive estimate of the hadronic top p_T as well as a discriminant against SM di-top events in which significant next-to-leading order effects of hard gluon emissions are non-negligible.

We pre-select the events which satisfy the following “Basic Cuts”:

$$p_T^{jR=1.0} > 500 \text{ GeV}, \quad \cancel{E}_T > 40 \text{ GeV}, \quad N_l^{out}(p_T^l > 25 \text{ GeV}) = 1, \\ N_j^{out}(p_T^j > 25 \text{ GeV}) \geq 1, \quad \Delta\phi_{jl} > 2.3, \quad \eta_{j,l} < 2.5, \quad (17)$$

where $p_T^{jR=1.0}$ is the transverse momentum of the hardest fat jet, $N_{l,j}^{out}$ is the number of leptons with $p_T > 25 \text{ GeV}$ and mini-ISO > 0.95 (l) [56] or anti- k_T $r = 0.4$ jets outside the fat jet (j), and $\Delta\phi_{jl}$ is the transverse plane angle between the fat jet and the lepton.

Our “leptonic top” candidate consists of the mini-isolated lepton, missing energy and a b -jet candidate, which we select to be the hardest $r = 0.4$ anti- k_T jet within the distance of $R = 1.5$ from the lepton.

We define our signal region with the following substructure cuts (in addition to Basic Cuts):

$$Ov_3^l > 0.5, \quad Ov_3^h > 0.5, \quad Ov_3^h + tPf > 1.0. \quad (18)$$

In addition, we only consider events with $m_{T\bar{T}} > 2.8, 3.5 \text{ TeV}$ for $M_{G'_{KK}} = 3, 5 \text{ TeV}$ respectively, where $m_{T\bar{T}}$ is the invariant mass of the leptonic and hadronic *peak templates*.

Table 7 summarizes our results for Case 1. TOM is able to improve S/B relative to the Basic Cuts by a factor of 10, while the signal significance improves by three-fold. The effect of 50 average pileup events is mild, with the apparent improvement in significance being due to the requirement on the lower p_T of the fat jet in the Basic Cuts. More background events pass the Basic Cuts in the presence of pileup but are efficiently rejected by TOM, thus causing a virtual improvement in the signal significance. The efficiency of the overlap cut on SM $t\bar{t}$ events is significantly lower than the signal $t\bar{t}$ events, due to the higher order effects becoming more prominent in high energy SM $t\bar{t}$ events.

We achieve significantly better sensitivity for higher masses at $L = 3000 \text{ fb}^{-1}$, with $S/\sqrt{B} \approx 4 - 5$ for $M_{G'_{KK}} = 5 \text{ TeV}$. Compared to 300 fb^{-1} , and $S/\sqrt{B} \approx 1.5$, we find that increasing luminosity in Case 1 could significantly improve the reach of the search.

Similarly, Table 8 summarizes our results for Case 2. We find that TOM again improves the signal significance by three-fold while S/B is improved by a factor of roughly 10. However, due to the lower signal cross section, neither the increase in luminosity to $L = 3000 \text{ fb}^{-1}$ nor TOM sufficiently improves the significance for $M_{G'_{KK}} = 5 \text{ TeV}$. Effects of pileup at 50 average interactions per bunch crossing are mild, with the results in S/B and S/\sqrt{B} being within 10%.

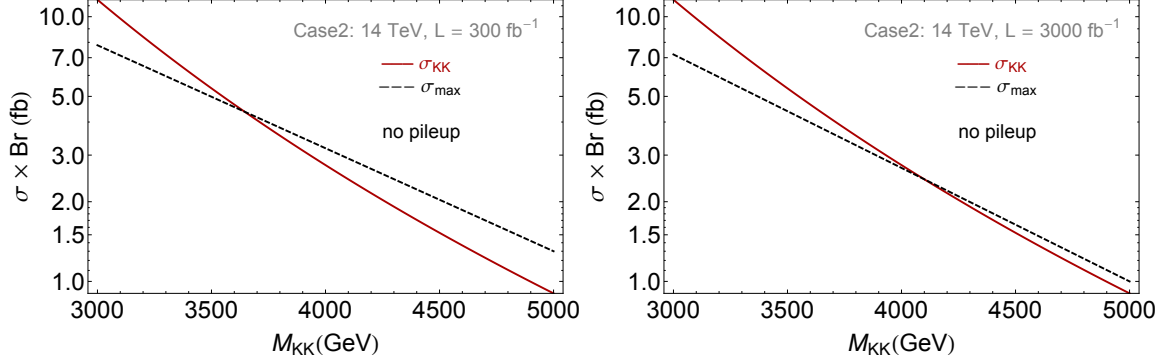


Figure 6: 95 % confidence level reach for the Case 2 KK gluon search at $\sqrt{s} = 14$ TeV with $L = 300, 3000 \text{ fb}^{-1}$. The dashed line represents the upper limit on the cross section whereas the solid line is the leading order KK gluon cross section.

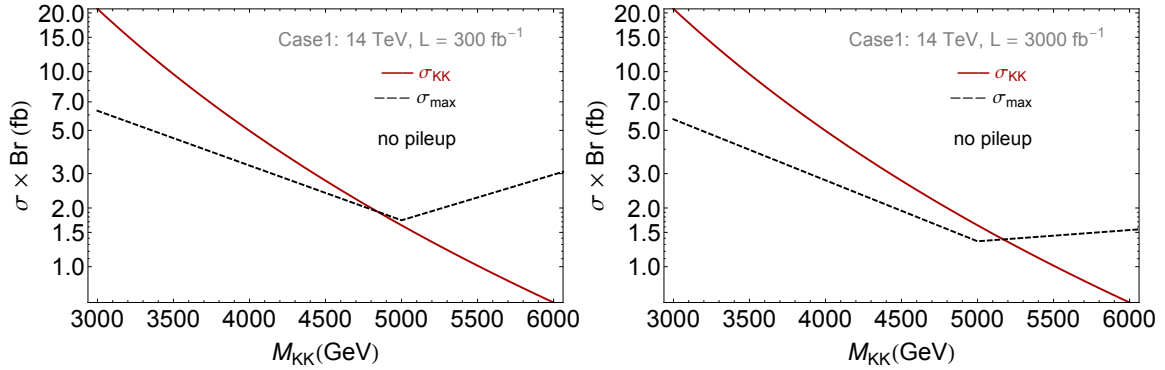


Figure 7: 95 % confidence level reach for the Case 1 KK gluon search at $\sqrt{s} = 14$ TeV with $L = 300, 3000 \text{ fb}^{-1}$. The dashed line represents the upper limit on the cross section whereas the solid line is the leading order KK gluon cross section.

We find that an increase in center of mass energy alone does not suffice to extend the experimental reach for the Case 2 KK gluon with mass $M_{G'_{\text{KK}}} = 5$ TeV. However, a combination of increase in \sqrt{s} to 33 TeV and the integrated luminosity of 3000 fb^{-1} can yield a 7σ signal as shown in Table 9.

Fig. 6 shows the results for the 95% CL sensitivity of the Case 2 KK gluon search at $\sqrt{s} = 14$ TeV and $L = 300, 3000 \text{ fb}^{-1}$. We include a 5% systematic uncertainty in the background into the calculation via a convolution with a log-normal distribution centered around the expected number of background events. We find that KK gluon masses up to ≈ 3.6 TeV can be excluded at $L = 300 \text{ fb}^{-1}$, and masses up to ≈ 4.1 TeV at $L = 3000 \text{ fb}^{-1}$.

Fig. 7 shows the corresponding sensitivity for the Case 1 KK gluon. We find that masses up to $M_{G'_{\text{KK}}} \approx 4.8$ TeV can be excluded at 14 TeV with 300 fb^{-1} , while the increase in luminosity to 3000 fb^{-1} only modestly improves the exclusion limit on $M_{G'_{\text{KK}}}$. Table 6 summarizes the results for $2\sigma, 3\sigma$ and 5σ reach.

Although the prospects for discovery of a KK gluon with mass of several TeV using jet substructure are good, the mass measurement is a more challenging task. Fig. 8 shows an illustration.

Luminosity	CL	Case 1	Case 2
300 fb^{-1}	2σ	4.8 TeV	3.6 TeV
	3σ	3.8 TeV	$< 3 \text{ TeV}$
	5σ	3.2 TeV	$< 3 \text{ TeV}$
3000 fb^{-1}	2σ	5.1 TeV	4.1 TeV
	3σ	4.4 TeV	3.5 TeV
	5σ	3.5 TeV	$< 3 \text{ TeV}$

Table 6: Mass reach of the $\sqrt{s} = 14 \text{ TeV}$ run search for RS KK gluons for 2, 3 and 5σ confidence intervals. All results include 5% systematics.

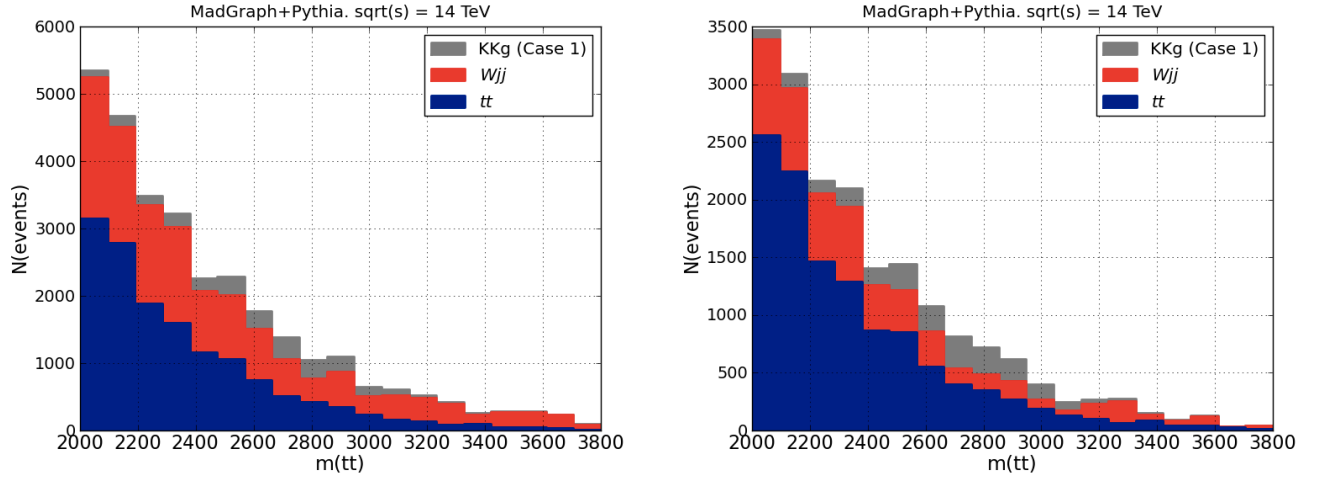


Figure 8: Invariant mass of the peak hadronic template and the peak leptonic template with basic cuts (left) and additional overlap cuts (right).

Strongly coupled resonances are typically characterized by large total decay widths, which in combination with the effects of PDF broadening result in a signal, which is smeared over a wide range of $m_{T\bar{T}}$. The mass measurement using a “bump fitting” technique will thus be challenging. Without the use of TOM, the measurement of $m_{T\bar{T}}$ is further complicated by the fact the Basic Cuts are sensitive to higher order effects (i.e. a hard gluon emission from a top quark) which further contribute to the smearing of the mass peak.

3.5 KK Z, γ [57]

Schematically, we get

$$q\bar{q} \rightarrow \text{KK } Z, \gamma \rightarrow WW, Zh \text{ (and } t\bar{t}, b\bar{b}) \quad (19)$$

There are actually three neutral KK states (generically denoted by Z'): KK photon (denoted by A_1), KK Z , and a KK mode of an extra $U(1)$ (again, with no corresponding zero-mode). The latter states mix after EWSB¹⁰ and the mass eigenstates are denoted by \tilde{Z}_1 and \tilde{Z}_{X_1} , where \tilde{Z}_1

¹⁰In obtaining the values of couplings shown below, this mixing is evaluated using 2 TeV KK mass: for more

Case 1, $\langle N_{vtx} \rangle = 0$, $M_{G'_{KK}} = 3$ TeV

Cuts	$\sigma_{t\bar{t}}(\text{fb})$	$\epsilon_{t\bar{t}}$	$\sigma_{Wjj}(\text{fb})$	ϵ_{Wjj}	σ_{KK}	ϵ_{KK}	S/B	$S/\sqrt{B}(300 \text{ fb}^{-1})$	$S/\sqrt{B}(3000 \text{ fb}^{-1})$
Basic Cuts	12.2	1.00	121.0	1.00	3.3	1.00	0.02	4.9	15.5
& $ Ov$ cuts	4.1	0.34	3.9	0.03	2.3	0.70	0.30	14.3	45.4

Case 1, $\langle N_{vtx} \rangle = 50$, $M_{G'_{KK}} = 3$ TeV

Cuts	$\sigma_{t\bar{t}}(\text{fb})$	$\epsilon_{t\bar{t}}$	$\sigma_{Wjj}(\text{fb})$	ϵ_{Wjj}	σ_{KK}	ϵ_{KK}	S/B	$S/\sqrt{B}(300 \text{ fb}^{-1})$	$S/\sqrt{B}(3000 \text{ fb}^{-1})$
Basic Cuts	18.7	1.00	208.5	1.00	4.1	1.00	0.02	4.7	14.9
& $ Ov$ cuts	5.2	0.25	5.2	0.025	2.9	0.70	0.30	15.7	49.0

Case 1, $\langle N_{vtx} \rangle = 0$, $M_{G'_{KK}} = 5$ TeV

Cuts	$\sigma_{t\bar{t}}(\text{fb})$	$\epsilon_{t\bar{t}}$	$\sigma_{Wjj}(\text{fb})$	ϵ_{Wjj}	σ_{KK}	ϵ_{KK}	S/B	$S/\sqrt{B}(300 \text{ fb}^{-1})$	$S/\sqrt{B}(3000 \text{ fb}^{-1})$
Basic Cuts	2.5	1.00	44.6	1.00	0.18	1.00	0.004	0.4	1.4
& $ Ov$ cuts	0.6	0.33	1.3	0.03	0.12	0.70	0.07	1.5	4.8

Case 1, $\langle N_{vtx} \rangle = 50$, $M_{G'_{KK}} = 5$ TeV

Cuts	$\sigma_{t\bar{t}}(\text{fb})$	$\epsilon_{t\bar{t}}$	$\sigma_{Wjj}(\text{fb})$	ϵ_{Wjj}	σ_{KK}	ϵ_{KK}	S/B	$S/\sqrt{B}(300 \text{ fb}^{-1})$	$S/\sqrt{B}(3000 \text{ fb}^{-1})$
Basic Cuts	4.2	1.00	73.0	1.00	0.18	1.00	0.002	0.4	1.1
& $ Ov$ cuts	0.9	0.27	2.0	0.027	0.12	0.69	0.041	1.3	4.1

Table 7: Results for Case 1 KK gluons with $M_{G'_{KK}} = 3, 5$ TeV, without and with $N_{vtx} = 50$ of pileup. The tables show the signal and background cross-sections at $\sqrt{s} = 14$ TeV with the corresponding signal significance at 300 fb^{-1} and 3000 fb^{-1} of integrated luminosity. The basic cuts include the pre-selections of Eq. 17 and a $m_{T\bar{T}} > 2.8$ TeV for $M_{G'_{KK}} = 3$ TeV, and $m_{T\bar{T}} > 3.5$ TeV for $M_{G'_{KK}} = 5$ TeV. The Ov cuts include additional cuts of Eq. 18. The apparent improved significance in the presence of pileup is due to the pileup sensitive lower p_T cut on the fat jet.

is “mostly” KK Z and \tilde{Z}_{X_1} is mostly the extra $U(1)$.

The dominant decay modes are to $t\bar{t}$, WW and Zh , each with a cross-section of $\sim O(10)$ fb for a 2 TeV Z' with a total decay width of ~ 100 GeV. However, the $t\bar{t}$ channel can be swamped by KK gluon $\rightarrow t\bar{t}$ if the Z' and KK gluon have similar mass.

The couplings relevant for production (for both cases I, II) are

	A_1	\tilde{Z}_{X_1}	\tilde{Z}_1
$u_L \bar{u}_L$	-0.04	-0.025	-0.046
$u_R \bar{u}_R$	-0.04	0.01	0.018
$d_L \bar{d}_L$	0.02	0.03	0.055
$d_R \bar{d}_R$	0.02	-0.005	0.0092

The notation used is that the coupling $Z u_L \bar{u}_L$ in SM is $g_Z (+1/2 - 2/3 \sin^2 \theta_W)$, with $g_Z \approx 0.74$, $\sin^2 \theta_W \approx 0.23$.

The decay into gauge bosons (for both cases I, II) is determined by

details of the dependence on KK mass, see references above.

Case 2: $\langle N_{vtx} \rangle = 0$, $M_{G'_{KK}} = 3$ TeV

Cuts	$\sigma_{t\bar{t}}$ (fb)	$\epsilon_{t\bar{t}}$	σ_{Wjj} (fb)	ϵ_{Wjj}	σ_{KK}	ϵ_{KK}	S/B	$S/\sqrt{B}(300 \text{ fb}^{-1})$	$S/\sqrt{B}(3000 \text{ fb}^{-1})$
Basic Cuts	12.2	1.00	121.0	1.00	1.38	1.00	0.01	2.1	6.6
& $ Ov$ cuts	4.1	0.34	3.9	0.03	1.02	0.74	0.13	6.3	19.8

Case 2: $\langle N_{vtx} \rangle = 0$, $M_{G'_{KK}} = 5$ TeV

Cuts	$\sigma_{t\bar{t}}$ (fb)	$\epsilon_{t\bar{t}}$	σ_{Wjj} (fb)	ϵ_{Wjj}	σ_{KK}	ϵ_{KK}	S/B	$S/\sqrt{B}(300 \text{ fb}^{-1})$	$S/\sqrt{B}(3000 \text{ fb}^{-1})$
Basic Cuts	2.5	1.00	44.6	1.00	0.17	1.00	0.001	0.3	0.8
& $ Ov$ cuts	0.6	0.33	1.3	0.03	0.12	0.72	0.01	0.7	2.3

Case 2: $\langle N_{vtx} \rangle = 50$, $M_{G'_{KK}} = 3$ TeV

Cuts	$\sigma_{t\bar{t}}$ (fb)	$\epsilon_{t\bar{t}}$	σ_{Wjj} (fb)	ϵ_{Wjj}	σ_{KK}	ϵ_{KK}	S/B	$S/\sqrt{B}(300 \text{ fb}^{-1})$	$S/\sqrt{B}(3000 \text{ fb}^{-1})$
Basic Cuts	18.7	1.00	208.5	1.00	1.6	1.00	0.007	1.8	5.8
& $ Ov$ cuts	5.2	0.25	5.2	0.025	1.2	0.74	0.11	6.3	20.0

Case 2: $\langle N_{vtx} \rangle = 50$, $M_{G'_{KK}} = 5$ TeV

Cuts	$\sigma_{t\bar{t}}$ (fb)	$\epsilon_{t\bar{t}}$	σ_{Wjj} (fb)	ϵ_{Wjj}	σ_{KK}	ϵ_{KK}	S/B	$S/\sqrt{B}(300 \text{ fb}^{-1})$	$S/\sqrt{B}(3000 \text{ fb}^{-1})$
Basic Cuts	4.2	1.00	73.0	1.00	0.17	1.00	7×10^{-4}	0.2	0.6
& $ Ov$ cuts	0.9	0.27	2.0	0.027	0.12	0.72	0.01	0.7	2.0

Table 8: Results for Case 2 KK gluons with $M_{G'_{KK}} = 3, 5$ TeV, without and with $N_{vtx} = 50$ of pileup. The tables show the signal and background cross-sections at $\sqrt{s} = 14$ TeV with the corresponding signal significance at 300 fb^{-1} and 3000 fb^{-1} of integrated luminosity. The basic cuts include the pre-selections of Eq. 17 and a $m_{T\bar{T}} > 2.8$ TeV for $M_{G'_{KK}} = 3$ TeV, and $m_{T\bar{T}} > 3.5$ TeV for $M_{G'_{KK}} = 5$ TeV. The Ov cuts include additional cuts of Eq. 18. The apparent improved significance in the presence of pileup is due to the pileup sensitive lower p_T cut requirement on the fat jet.

Case 2: $\langle N_{vtx} \rangle = 0$, $M_{G'_{KK}} = 5$ TeV

Cuts	$\sigma_{t\bar{t}}$ (fb)	$\epsilon_{t\bar{t}}$	σ_{Wjj} (fb)	ϵ_{Wjj}	σ_{KK}	ϵ_{KK}	S/B	$S/\sqrt{B}(300 \text{ fb}^{-1})$	$S/\sqrt{B}(3000 \text{ fb}^{-1})$
Basic Cuts	173.0	1.00	800.0	1.00	2.16	1.00	0.002	1.2	3.7
& $ Ov$ cuts	48.0	0.28	39.0	0.04	1.26	0.58	0.01	2.4	7.4

Table 9: Results for Case 2 KK gluons with $M_{G'_{KK}} = 5$ TeV. The table shows the signal and background cross-sections at $\sqrt{s} = 33$ TeV with the corresponding signal significance at 300 fb^{-1} and 3000 fb^{-1} of integrated luminosity. The basic cuts include the pre-selections of Eq. 17 and $m_{T\bar{T}} > 3.5$ TeV for $M_{G'_{KK}} = 5$ TeV. The Ov cuts include additional cuts of Eq. 18.

	A_1	\tilde{Z}_{X_1}	\tilde{Z}_1
WW	-0.0062	-0.0069	-0.0078
Zh	0	-67.3 GeV	482 GeV

where the notation used is that the couplings γWW and ZWW in SM are $-g \sin \theta_W$ and $-g \cos \theta_W$ (respectively), with $g \approx 0.65$.

Finally, the decays to SM fermions are given by

	A_1	\tilde{Z}_{X_1}	\tilde{Z}_1
$t_L \bar{t}_L$	0.21	-0.32	0.47
$b_L \bar{b}_L$	-0.1	-0.6	-0.03
$t_R \bar{t}_R$	0.81	-0.77	-0.085

and

	A_1	\tilde{Z}_{X_1}	\tilde{Z}_1
$t_L \bar{t}_L$	0.81	-1.05	1.72
$b_L \bar{b}_L$	-0.4	-2.1	-0.24
$t_R \bar{t}_R$	0.21	-0.22	-0.008

for both cases I, II, respectively.

Having summarized the couplings of KK Z , γ , we now move on to two specific searches that were studied as part of the Snowmass 2013 process.

3.5.1 KK $Z \rightarrow ZH$

Samples of 10,000 signal events are generated using our implementation of the model in CalcHEP [58] with the first KK excitation Z_{KK} forced to decay to the ZH final state. Z_{KK} masses of 2 and 3 TeV are chosen and the corresponding cross sections are shown in Table 10. For background processes, Z +jets events are generated with MadGraph 5.11 [33] and Pythia 6.420 [35] for parton shower and hadronization. Those events are produced separately for one- and two-jet topologies, and light vs. heavy flavors, see Table 11. A minimum p_T requirement is imposed on the dilepton pair to enhance the available integrated luminosity in the final signal region with a lower (higher) minimum value for the study of 2 (3) TeV Z_{KK} , corresponding to the upper (lower) portions of Table 11.

Table 10: Cross sections for signal processes in pp collisions at $\sqrt{s} = 14$ TeV.

Process	mass [TeV]	cross section [fb]	# events
$pp \rightarrow Z_{KK} \rightarrow ZH$	2.0	19.1	10,000
$pp \rightarrow Z_{KK} \rightarrow ZH$	3.0	2.40	10,000

Signal samples are processed through Pythia 8.176 [24] to produce parton showers and hadronize partons. Final decays $Z \rightarrow e^+e^-$, $Z \rightarrow \mu^+\mu^-$ and $H \rightarrow b\bar{b}$ are forced at this stage with a Higgs mass set to 125 GeV. For the data analysis described below the following branching ratios are

Table 11: Cross sections for background processes in pp collisions at $\sqrt{s} = 14$ TeV. Jets j include the following particles: $g, u, \bar{u}, d, \bar{d}, s, \bar{s}, c, \bar{c}$. The $pp \rightarrow Zb$ process includes both Zb and $Z\bar{b}$ final states.

Process	min $p_T^{\ell\ell}$ [TeV]	cross section [fb]	# events
$pp \rightarrow Zj$	0.5	72.6	100,000
$pp \rightarrow Zjj$	0.5	132	100,000
$pp \rightarrow Zb$	0.5	1.40	50,000
$pp \rightarrow Zb\bar{b}$	0.4	4.51	50,000
$pp \rightarrow Zj$	0.7	13.0	100,000
$pp \rightarrow Zjj$	0.7	25.1	80,000
$pp \rightarrow Zb$	0.7	0.172	50,000
$pp \rightarrow Zb\bar{b}$	0.7	0.222	50,000

assumed: $BR(Z \rightarrow \ell^+\ell^-) = 0.067$ and $BR(H \rightarrow b\bar{b}) = 0.588$. Detector simulation is performed with Delphes 3.0.9 [26] including the effects of 50 pileup collisions.

Signal event candidates are selected based on the following object requirements:

- Electrons and muons have transverse momentum $p_T > 25$ GeV and pseudorapidity $|\eta| < 2.5$;
- Both are required to be isolated from other tracks in the event, i.e. the ratio between the sum of transverse momenta of track within a cone of $\Delta R = \sqrt{(\Delta\eta)^2 + (\Delta\phi)^2} = 0.3$ and the lepton p_T and is less than 10%: $\Sigma p_T^{\text{tracks}}/p_T < 0.1$, where the sum excludes all leptons of the same flavor as the candidate lepton; this is done to avoid removing $Z \rightarrow \ell\ell$ decays with a highly boosted lepton pair;
- Jets reconstructed with the anti- k_t algorithm with a distance parameter of 0.5 must have $p_T > 100$ GeV and $|\eta| < 2.5$;
- Jets must pass the loose b -tag requirements.

Z candidates are formed from pairs of same-flavor leptons without any requirement on their electric charge. In case there are more than one candidate in each event, a single candidate is chosen by selecting the lepton pair with mass closest to the Z boson mass. Finally, this pair is required to have a mass within 15 GeV of the Z boson mass. The above selection has an efficiency of about 40% for signal events.

H candidates are identified from the set of b -tagged jets with a jet mass within 20 (25) GeV of the Higgs boson mass for a Z_{KK} mass of 2 (3) TeV, respectively. With a distance parameter $R = 0.5$, $H \rightarrow b\bar{b}$ final state particles are expected to be merged into a single jet. For example, a Higgs boson with $p_T = 1$ TeV would produce two b quarks with an angular separation $\Delta R = 2m_H/p_T = 0.25$. Jet mass distributions for signal decays of 2 and 3 TeV masses are presented in Fig. 9. The jet selection is about 31% (33%) efficient for signal events.

Finally, ZH candidates must pass the following requirements:

- Z candidate $p_T > 500$ GeV;
- H candidate $p_T > 500$ GeV;
- cosine of the angle between the Z and H candidate momentum vectors is less than -0.5 ;

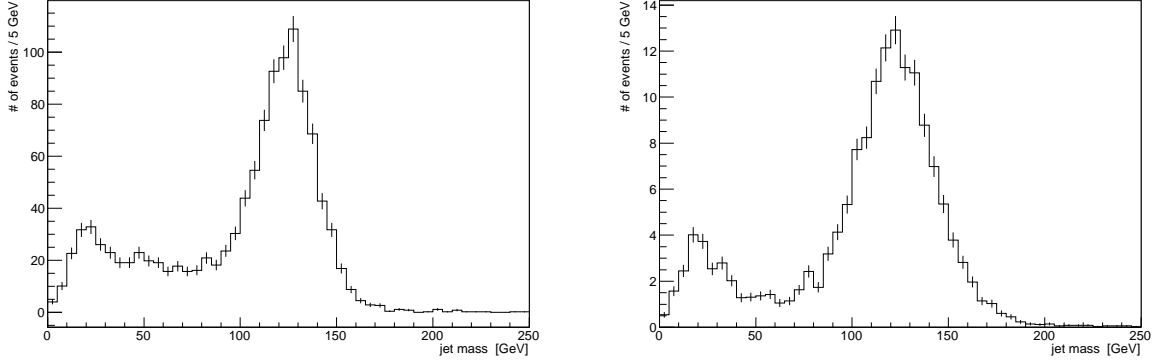


Figure 9: Mass distribution for jets passing the initial selection: $p_T > 100$ GeV, $|\eta| < 2.5$, and loose b tag, for signal events with Z_{KK} mass of 2 TeV (left) and 3 TeV (right).

- ZH mass is within 200 (300) GeV of the target Z_{KK} mass for the 2 (3) TeV Z_{KK} cases.

The overall acceptance times efficiency for the full selection is about 12% (14%) for Z_{KK} mass of 2 (3) TeV.

Figs. 10 and 11 show the mass distributions for the ZH candidates passing all selection criteria, except the final mass window cut, in the Z_{KK} mass = 2 (3) TeV cases, respectively.

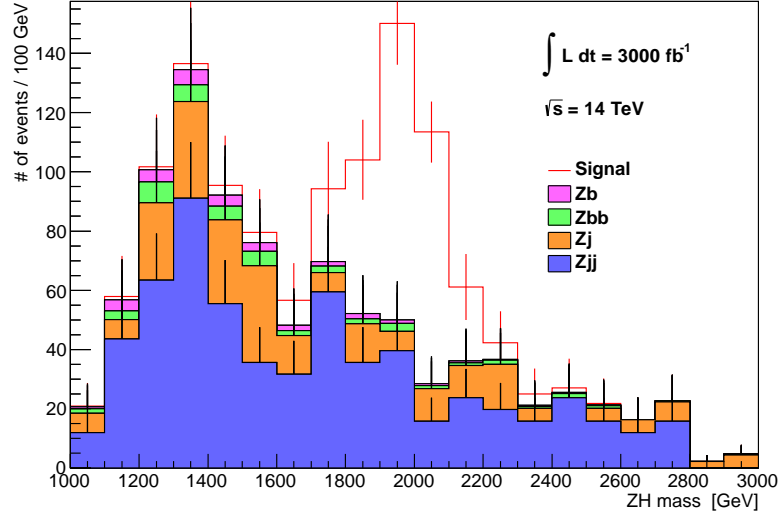


Figure 10: Mass distribution for ZH candidates passing the selection criteria for the Z_{KK} mass of 2 TeV, except for the mass requirement.

Table 12 presents the signal and background event yields after all selection requirements listed above are applied. Both 2 and 3 TeV mass points can be observed with significance (S/\sqrt{B}) above 5σ with an integrated luminosity of 3000 fb^{-1} . For the 2 TeV case, 300 fb^{-1} would be sufficient for a discovery with a significance of 6.1.

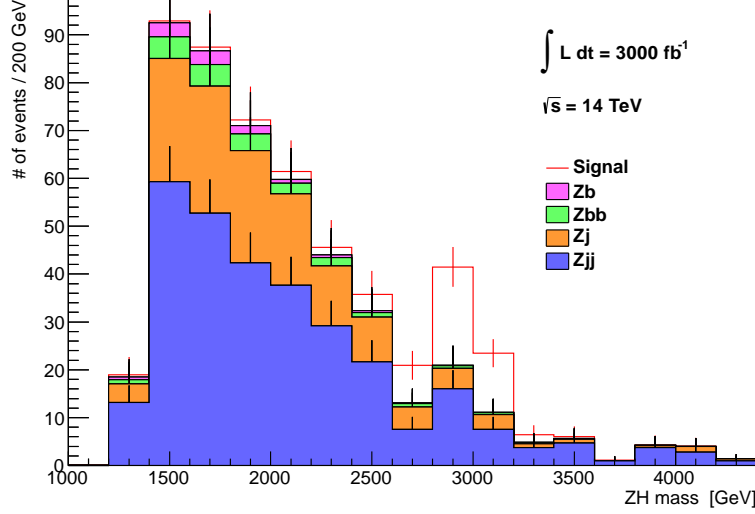


Figure 11: Mass distribution for ZH candidates passing the selection criteria for the Z_{KK} mass of 3 TeV, except for the mass requirement.

Table 12: Event yields for signal and background processes in pp collisions at $\sqrt{s} = 14$ TeV with 3000 fb^{-1} of integrated luminosity.

Process	Z_{KK} mass = 2 TeV	Z_{KK} mass = 3 TeV
$pp \rightarrow Z_{KK} \rightarrow ZH$	264.2 ± 7.7	39.3 ± 1.1
$pp \rightarrow Zj$	50 ± 10	10.5 ± 2.0
$pp \rightarrow Zjj$	123 ± 22	28 ± 5
$pp \rightarrow Zb$	4.3 ± 0.6	0.32 ± 0.06
$pp \rightarrow Zb\bar{b}$	6.2 ± 1.3	1.49 ± 0.14
Total background	183 ± 24	40.6 ± 5.5
Signal significance	19.5	6.2

3.5.2 Reinterpretation of the search for narrow $t\bar{t}$ resonances

The search for narrow $t\bar{t}$ resonances in the all-hadronic final state described in Sec. 3.2 is reinterpreted in terms of limits on KK Z' and Z_1 bosons decaying to $t\bar{t}$. Tab. 13 shows the signal cross sections used in the reinterpretation. The k -factor of 1.3 used in the leptophobic top-color Z' analysis is also used here, although it has only limited validity in this scenario.

Fig. 12 shows the 95% CL limits on the cross section of a narrow resonance overlaid with the expected cross sections for the KK models. The mass limits for the KK Z' boson are given in Tab. 14 for the different pile-up and luminosity scenarios for statistical uncertainties only and with systematic uncertainties included. If the mass limit is denoted < 2 TeV, the analysis is not sensitive to resonance mass above 2 TeV. No mass limits are given for the Z_1 boson given the low predicted cross section for this process. With 3000 fb^{-1} of data at 14 TeV, KK Z' bosons can be excluded with masses up to 2.8 TeV using this analysis in the all-hadronic $t\bar{t}$ decay channel.

Table 13: Cross sections at 14 TeV considered in the analysis of the search for narrow $t\bar{t}$ resonances.

scenario	Z_{KK} mass	cross section
KK Z'	2 TeV	17.2 fb
KK Z'	3 TeV	1.8 fb
KK Z'	4 TeV	0.31 fb
KK Z'	5 TeV	0.075 fb
KK Z_1	2 TeV	3.43 fb
KK Z_1	3 TeV	0.42 fb
KK Z_1	4 TeV	0.074 fb
KK Z_1	5 TeV	0.017 fb

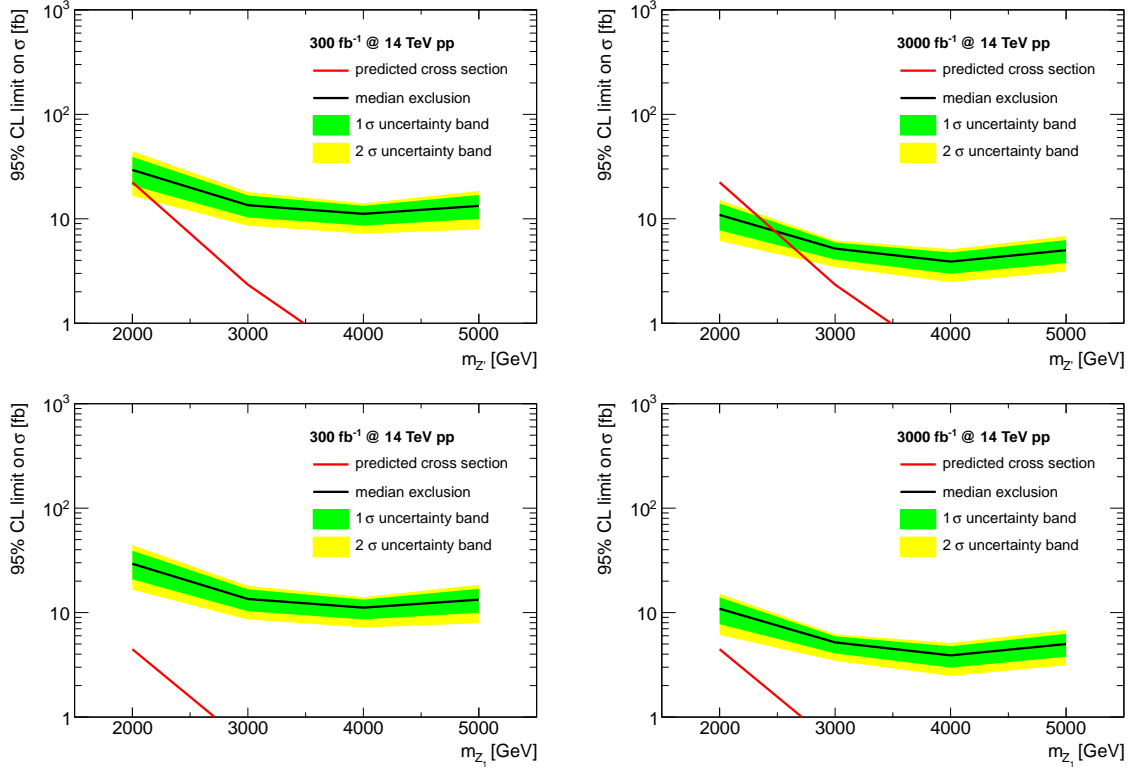


Figure 12: Expected cross section upper limits at 95% CL for the KK Z' and Z_1 models (upper and lower plots) decaying to a top quark pair in the all-hadronic channel. The left plots show the limits for 300 fb $^{-1}$ of 14 TeV data and $\mu = 50$. The right plots show the limits for 3000 fb $^{-1}$ of data and $\mu = 140$ (right).

3.6 KK W [22]

Here, we get

$$q'\bar{q} \rightarrow \text{KK } W \rightarrow WZ, Wh(\text{and } t\bar{b}) \quad (20)$$

It turns out that in addition to KK W_L^+ , these models also have a KK W_R^+ (with no corresponding zero-mode), due to the custodial (i.e., extended 5D gauge) symmetry. These two KK states mix after EWSB and the mass eigenstates are denoted by \tilde{W}_{L1}^+ and \tilde{W}_{R1}^+ , with former being

Table 14: 95% CL limits on the resonance mass for the KK Z' model decaying to a top quark pair in the all-hadronic channel. Limits are given for pile-up scenarios and integrated luminosities.

scenario	lumi.	pile-up	uncertainties	mass reach
KK Z'	300 fb $^{-1}$	$\mu = 0$	stat.	2.6 TeV
KK Z'	300 fb $^{-1}$	$\mu = 0$	stat.+syst.	< 2 TeV
KK Z'	300 fb $^{-1}$	$\mu = 50$	stat.	2.6 TeV
KK Z'	300 fb $^{-1}$	$\mu = 50$	stat.+syst.	< 2 TeV
KK Z'	300 fb $^{-1}$	$\mu = 140$	stat.	2.5 TeV
KK Z'	300 fb $^{-1}$	$\mu = 140$	stat.+syst.	< 2 TeV
KK Z'	3000 fb $^{-1}$	$\mu = 0$	stat.	3.3 TeV
KK Z'	3000 fb $^{-1}$	$\mu = 0$	stat.+syst.	2.9 TeV
KK Z'	3000 fb $^{-1}$	$\mu = 50$	stat.	3.2 TeV
KK Z'	3000 fb $^{-1}$	$\mu = 50$	stat.+syst.	2.9 TeV
KK Z'	3000 fb $^{-1}$	$\mu = 140$	stat.	3.2 TeV
KK Z'	3000 fb $^{-1}$	$\mu = 140$	stat.+syst.	2.8 TeV

mostly KK W_L^+ . The dominant decay modes for W' (generic notation) are into WZ and Wh . For a 2 TeV W' , the cross-section $\sim O(10)$ fb each with a total decay width of $\sim O(100)$ GeV. In some models, W' decays to $t\bar{b}$ – giving boosted top and bottom – can also have similar cross-section. Interestingly, the process KK gluon $\rightarrow t\bar{t}$ – with KK gluon mass being similar to W' – can be a significant background to this channel since a highly boosted top quark can fake a bottom quark: techniques similar to the ones used to identify highly boosted tops can now be applied to *veto* this possibility!

The production (for both cases I and II) goes via

	$\tilde{W}_{L_1}^+$	$\tilde{W}_{R_1}^+$
$d_L \bar{u}_L$	-0.074	-0.055

where the notation used is that the coupling $d_L \bar{u}_L W$ in SM is $g/\sqrt{2}$.

The decay to gauge bosons (for both cases I and II) depend on

	$\tilde{W}_{L_1}^+$	$\tilde{W}_{R_1}^+$
WZ	-0.0026	-0.0182
Wh	429 GeV	-61.3 GeV

while that to SM fermions are given by

	$\tilde{W}_{L_1}^+$	$\tilde{W}_{R_1}^+$
$b_L \bar{t}_L$	0.37	0.28

for case I and

	$\tilde{W}_{L_1}^+$	$\tilde{W}_{R_1}^+$
$b_L \bar{t}_L$	1.44	1.08

for case II.

Next, we describe a study of a specific decay channel for KK W .

3.6.1 KK $W \rightarrow Wh$

The discovery potential of the KK W_L^+ at the 3000 fb $^{-1}$ LHC is studied using the Wh decay channel where W bosons decays leptonically and H bosons decaying to $b\bar{b}$. The signal samples are generated using our implementation of the model in **CalcHep 3.4.2** [58]. The W +jets and $t\bar{t}$ events, the dominant SM background processes, are simulated with **Madgraph 5.11** [33]. Both signal and background events are then passed to **Pythia 6.420** [35] for showering and hadronization. The **Delphes 3.0.9** [26] program is used with Snowmass fast detector simulation settings for object reconstruction. Note that this study was done without pile-up. However, because of the high kinematic cuts we applied we expect that it should be relatively insensitive to pile-up effects.

For high KK W_L^+ masses, the produced Higgs bosons are highly boosted and the two bottom quarks from the hadronically decaying Higgs boson are expected to be reconstructed as one jet due to limited hadronic calorimeter resolution. Thus the final state topology consists of one isolated lepton (e or μ), large transverse missing energy and one highly energetic massive jet. The events are selected using the following criteria:

- one and only one lepton: $p_T^l > 25$ GeV, $|\eta^l| < 2.5$, $\Sigma p_T^{tracks}/p_T < 0.1$
- one and only one b-jet: $p_T^j > 30$ GeV, $|\eta^j| < 2.5$, loose b-tag
- transverse missing energy > 200 GeV.

The lepton is either electron or muon and the track isolation criteria is calculated within distance parameter 0.3. The jets are reconstructed using the anti- k_t algorithm with a distance parameter 0.5. The DELPHES loose b-tag efficiency is applied; it corresponds to 80% efficiency for b-jets and 6% efficiency for light jets. The one and only one b-jet selection can significantly reduce the top background which usually produces multiple b-jets.

To further improve the signal purity, the additional Higgs candidate selection is applied to the jet:

- $p_T^j > 1000 + (M_{KKW} - 3000)/2$ GeV,
- 100 GeV $< m_j < 150$ GeV.

This selection is based on the fact that the Higgs decaying from the KK W_L^+ is highly boosted with large transverse momentum and so the jet, with distance parameter $R=0.5$, is expected to contain both decayed b-quarks.

Finally, the KK W candidate must pass the following additional criteria:

- W candidate $p_T > 500$ GeV,
- $|\phi_l - \phi_{missing\ E_T}| < 1$,
- $|\phi_l - \phi_j| > 2.5$.

- $2.4 \text{ TeV} < m_{W,H} < 3.2 \text{ TeV}$ ($2.9 \text{ TeV} < m_{W,H} < 4.1 \text{ TeV}$) for the 3 (4) TeV W_{KK} cases.

The $\phi_{l,\nu}$ selection is based on the fact that the W is highly boosted and so the lepton and neutrino are expected to be highly collimated. The angle between the lepton and the missing energy in the xy-plane should be small. Furthermore, since the KK W has little transverse momentum, we expect the angle between the W and Higgs, and therefore the lepton and jet, in the xy-plane to be very large.

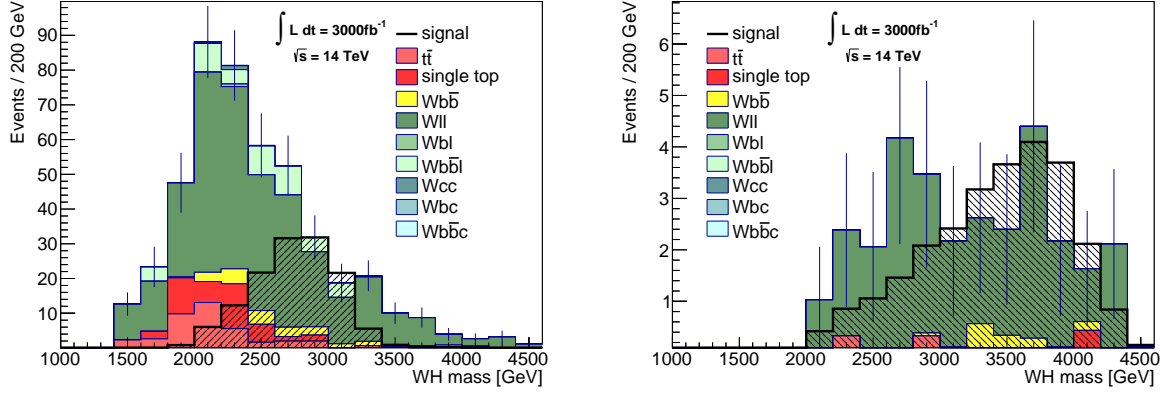


Figure 13: The invariant mass distribution for the KK W_L^+ of mass 3 TeV (left) and 4 TeV (right) at $\sqrt{s} = 14 \text{ TeV}$ in the decay channel $pp \rightarrow W_L^+ \rightarrow Wh \rightarrow l^+ \nu b \bar{b}$. The neutrino momentum is resolved using a W mass constraint.

Fig.13 shows the invariant mass distribution of KK W_L^+ in the decay channel $pp \rightarrow \text{KK } W \rightarrow Wh \rightarrow l \nu b \bar{b}$ at the $\sqrt{s} = 14 \text{ TeV}$. The W mass constraint is used to resolve the z-momentum component of the neutrino assuming it is the only source of the missing energy. The higher $|p_z^{\nu}|$ solution is selected from this quadratic equation although both solutions give similar $M_{l\nu b \bar{b}}$ distributions.

Table 15 presents the expected yields and observation significance at 3000 fb^{-1} 14 TeV collisions. The signal region is selected about one sigma of the mass resolution for each KK W_L^+ search hypothesis. The mass resolution is driven 50% from the natural width and another 50% from the detector resolution. The observation significance of the 3 TeV (4 TeV) KK W_L^+ is 5.4 (3.5) σ .

Process	$M_{\text{KK}W_L^+} = 3 \text{ TeV}$	$M_{\text{KK}W_L^+} = 4 \text{ TeV}$
w + light jets	112.2 ± 10.7	13.4 ± 3.7
w + mixed jets	25.2 ± 10.1	-
w + heavy jets	10.2 ± 0.7	1.6 ± 0.3
$t\bar{t}$	5.6 ± 1.4	-
single top	8.2 ± 3.4	0.4 ± 0.4
total background	161.4 ± 15.2	15.4 ± 3.8
signal	106.7 ± 3.0	19.2 ± 0.6
significance	5.4	3.5

Table 15: In the $pp \rightarrow \text{KK}W_L^+ \rightarrow l\nu b \bar{b}$ process, the expected yields of signal and background process and the observation significance.

3.7 Heavier KK fermions [21]

The KK fermions in the minimal model being 2 TeV or heavier, even single production of these particles can be very small (pair production is even smaller).

3.8 Light KK fermions (a.k.a. “Top partners”) [59]

As mentioned above, in non-minimal models, KK partners of top/bottom can be light so that their production (both pair and single, the latter perhaps in association with SM particles) can be significant. As these particles are “top-like” with respect to their production at the LHC, the yields can be sizeable. For example, the pair production cross-section of a KK bottom with mass of 500 GeV is ~ 1 pb at $\sqrt{s} = 10$ TeV. These particles decay into $t/b + W/Z/h$, where the W/Z can be somewhat boosted at the LHC (even for fermionic KK partners with masses as low as ~ 500 GeV). Some of these light KK fermions can have “exotic” electric charges – for example, $4/3$ and $5/3$. This makes them appealing with respect to a generic b'/t' from, for example, a minimal extension of the number of SM generations. For details, see references given above and Snowmass 2013 studies of “Heavy fermions” under simplified models [60].

In addition, the other heavier (spin-1 or 2) KK modes can decay into these light KK fermions, resulting in perhaps more distinctive final states for the heavy KK’s than the pairs of W/Z or top quarks that have been studied so far – for such a study for KK gluon, see reference [61].

4 Indirect KK effects

In addition to signals from the *direct* production of the KK particles at the LHC, there can also be effects from virtual exchange of these KK particles on the properties of the SM particles themselves. Again, details are given in the references.

4.1 Top couplings to gauge bosons

The shift in coupling of top quark to Z , *relative* to that in the SM, is given by (section 4.1 of [62])

$$\begin{aligned}\delta(Zt\bar{t}) &\sim \frac{g_Z^2 k \pi r_c v^2}{M_{\text{KK}}^2}, \frac{Y_5^2 v^2}{M_{\text{KK}}^2} \\ &\lesssim 10\%, \text{ for } M_{\text{KK}} \gtrsim \text{a few TeV}\end{aligned}\tag{21}$$

Here, Y_5 denotes 5D Yukawa coupling in units of k . Note that this holds for either RH or LH top quark, depending on case I or II, thereby allowing for experimental distinction between the two cases.

Similarly, we have

$$\begin{aligned}\delta(Wt\bar{b}) &\sim \frac{g^2 k \pi r_c v^2}{M_{\text{KK}}^2}, \frac{Y_5^2 v^2}{M_{\text{KK}}^2} \\ &\lesssim 10\%, \text{ for } M_{\text{KK}} \gtrsim \text{a few TeV}\end{aligned}\tag{22}$$

but only for case II (i.e., LH top/bottom being localized close to the TeV brane).

4.2 Top-Higgs coupling

The shift is given by [63]:

$$\delta(ht\bar{t}) \sim \frac{Y_5^2 v^2}{M_{\text{KK}}^2} \quad (23)$$

4.3 Higgs couplings to gauge bosons

The shifts in Higgs couplings to W , Z are as above for top quark (1st term there only). For massless gauge bosons, we get [64]:

$$\delta(hgg, h\gamma\gamma) \sim \frac{Y_5^2 v^2}{M_{\text{KK}}^2} \quad (24)$$

It turns out that the above shifts (especially the latter ones) are [mostly $O(1)$] different [65] for the case of “gauge-Higgs unification” (where the Higgs boson is realized as A_5 [9]) as compared to the model where it is a mode of a $5D$ scalar field.

4.4 Triple -gauge-couplings

We estimate:

$$\begin{aligned} \delta(WWZ) &\sim \frac{g_Z^2 v^2}{M_{\text{KK}}^2} \\ &\lesssim 0.1\%, \text{ for } M_{\text{KK}} \gtrsim \text{a few TeV} \end{aligned} \quad (25)$$

the smallness of which is related (perhaps as expected in most theories) to that of precision EW observables (such as the S parameter).

5 Additional considerations

Note that in general, brane-localized kinetic terms for $5D$ fields are allowed [66], but we have assumed them to be negligible here. Similarly, the metric can deviate from pure AdS_5 near TeV brane [67]. Both these cases result in $O(1)$ variations (relative to the above framework) of the phenomenology. And, the UV-IR hierarchy can be from flavor scale (only) of ~ 1000 ’s of TeV to EW scale [68]. In this case, the phenomenology is qualitatively similar, but can be different by more than $O(1)$.

The really/qualitatively different modifications are as follows.

5.1 Flavor

As mentioned above, we do need flavor symmetries to allow a few TeV KK scale to be consistent with the relevant precision tests. The signals outlined above are largely independent of the details of this implementation; of course, any flavor-*violating* signals will depend on it. In addition, flavor symmetries can allow the possibility of light fermions being localized near the TeV brane (while not explaining the flavor hierarchy as outlined in the above framework). For these details, see companion note [15].

5.2 Dark Matter

There is no candidate for dark matter (DM) in the minimal model presented above, for example, there is no KK-parity (unlike in UED).

However, in a well-motivated extension, it turns out that a DM candidate emerges naturally¹¹. Namely, when we incorporate a GUT into the above framework, then suppressing proton decay gives a weakly-interacting massive particle (WIMP) DM candidate as a spin-off [8]. In this model, in addition to DM, there are (as is usual in WIMP models in general) *other* states charged under Z_3 , but which are also charged SM: these have to decay into DM, plus SM: see section 15 of 2nd reference in [8]. In particular, the DM stabilization symmetry is Z_3 (cf. Z_2 in UED or SUSY), which can have interesting consequences for DM signals: see references [70] for studies of this kind (in general).

5.3 Gauge-Higgs unification

Since this involves a further extension of the EW gauge symmetry, one obtains extra spin-1 particles, but these are typically heavier: see [71] for a study¹².

6 Summary

The framework of warped extra dimension is a well-motivated extension of the SM. In this whitepaper prepared for the Snowmass 2013 process, we have described searches at the LHC for the spin-1 and spin-2 KK particles in this framework. We find that the prospects for discovery of these particles are quite promising, especially at the high-luminosity upgrade.

Acknowledgments: This work was supported in by the following grants (with respective authors): NSF Grant No. PHY-0968854 (KA), Danish National Research Foundation under the contract number DNRF90 (OA), Alexander von Humboldt Foundation under “sgrants” (JE), the Department of Energy Office of Science and the Alfred P. Sloan Foundation and the Research Corporation for Science Advancement (TG), National Research Foundation of Korea(NRF) grant funded by the Korea government(MEST) N01120547 (SJL).

References

- [1] L. Randall and R. Sundrum, Phys. Rev. Lett. **83**, 3370 (1999) [arXiv:hep-ph/9905221].
- [2] H. Davoudiasl, J. L. Hewett and T. G. Rizzo, Phys. Lett. B **473**, 43 (2000) [arXiv:hep-ph/9911262]; A. Pomarol, Phys. Lett. B **486**, 153 (2000) [arXiv:hep-ph/9911294]; S. Chang, J. Hisano, H. Nakano, N. Okada and M. Yamaguchi, Phys. Rev. D **62**, 084025 (2000) [arXiv:hep-ph/9912498].
- [3] Y. Grossman and M. Neubert, Phys. Lett. B **474**, 361 (2000) [arXiv:hep-ph/9912408].
- [4] T. Gherghetta and A. Pomarol, Nucl. Phys. B **586**, 141 (2000) [arXiv:hep-ph/0003129].
- [5]

¹¹The other possibility is to add a sector to the minimal model just for obtaining a DM candidate [69].

¹²One also gets extra KK fermions which can result in quantitative changes to the phenomenology.

- [6] H. Davoudiasl, S. Gopalakrishna, E. Ponton and J. Santiago, arXiv:0908.1968 [hep-ph].
- [7] K. Agashe, R. Contino and R. Sundrum, Phys. Rev. Lett. **95**, 171804 (2005) [arXiv:hep-ph/0502222].
- [8] K. Agashe and G. Servant, Phys. Rev. Lett. **93**, 231805 (2004) [arXiv:hep-ph/0403143] and JCAP **0502**, 002 (2005) [arXiv:hep-ph/0411254].
- [9] R. Contino, Y. Nomura and A. Pomarol, Nucl. Phys. B **671**, 148 (2003) [arXiv:hep-ph/0306259]; K. Agashe, R. Contino, A. Pomarol, Nucl. Phys. B **719**, 165 (2005) [hep-ph/0412089].
- [10] W. D. Goldberger and M. B. Wise, Phys. Rev. Lett. **83**, 4922 (1999) [arXiv:hep-ph/9907447]; J. Garriga and A. Pomarol, Phys. Lett. B **560**, 91 (2003) [arXiv:hep-th/0212227].
- [11] J. M. Maldacena, Adv. Theor. Math. Phys. **2**, 231 (1998) [Int. J. Theor. Phys. **38**, 1113 (1999)] [arXiv:hep-th/9711200]; S. S. Gubser, I. R. Klebanov and A. M. Polyakov, Phys. Lett. B **428**, 105 (1998) [arXiv:hep-th/9802109]; E. Witten, Adv. Theor. Math. Phys. **2**, 253 (1998) [arXiv:hep-th/9802150].
- [12] N. Arkani-Hamed, M. Porrati and L. Randall, JHEP **0108**, 017 (2001) [arXiv:hep-th/0012148]; R. Rattazzi and A. Zaffaroni, JHEP **0104**, 021 (2001) [arXiv:hep-th/0012248].
- [13] C. Delaunay, O. Gedalia, S. J. Lee, G. Perez and E. Ponton, Phys. Rev. D **83**, 115003 (2011) [arXiv:1007.0243 [hep-ph]]; C. Delaunay, O. Gedalia, S. J. Lee, G. Perez and E. Ponton, Phys. Lett. B **703**, 486 (2011) [arXiv:1101.2902 [hep-ph]].
- [14] S. J. Huber, Nucl. Phys. B **666**, 269 (2003) [arXiv:hep-ph/0303183]; K. Agashe, G. Perez and A. Soni, Phys. Rev. D **71**, 016002 (2005) [arXiv:hep-ph/0408134].
- [15] Go to the link: <https://www.dropbox.com/s/aidq5fn2lp8ljwj/snowmassWarpedBenchmarks.pdf>
- [16] K. Agashe, A. Delgado, M. J. May and R. Sundrum, JHEP **0308**, 050 (2003) [arXiv:hep-ph/0308036].
- [17] K. Agashe, R. Contino, L. Da Rold and A. Pomarol, Phys. Lett. B **641** (2006) 62 [arXiv:hep-ph/0605341].
- [18] M. Carena, E. Ponton, J. Santiago and C. E. M. Wagner, Nucl. Phys. B **759**, 202 (2006) [arXiv:hep-ph/0607106] and Phys. Rev. D **76**, 035006 (2007) [arXiv:hep-ph/0701055].
- [19] See, for example, Y. Eshel, S. J. Lee, G. Perez, Y. Soreq JHEP **1110**, 015 (2011) [arXiv:1106.6218 [hep-ph]].
- [20] A. Altheimer, S. Arora, L. Asquith, G. Brooijmans, J. Butterworth, M. Campanelli, B. Chapeau and A. E. Cholakian *et al.*, J. Phys. G **39**, 063001 (2012) [arXiv:1201.0008 [hep-ph]].
- [21] H. Davoudiasl, T. G. Rizzo and A. Soni, Phys. Rev. D **77**, 036001 (2008) [arXiv:0710.2078 [hep-ph]].
- [22] K. Agashe, S. Gopalakrishna, T. Han, G. Y. Huang and A. Soni, arXiv:0810.1497 [hep-ph].
- [23] R. M. Harris, C. T. Hill and S. J. Parke, [hep-ph/9911288].

- [24] T. Sjöstrand, S. Mrenna and P. Skands, *Comput. Phys. Commun.* **178** 852 (2008), [arXiv:0710.3820].
- [25] M. Bahr *et al.*, *Eur. Phys. J. C* **58**, 639 (2008), [arXiv:0803.0883].
- [26] J. de Favereau, C. Delaere, P. Demin, A. Giammanco, V. Lematre, A. Mertens and M. Selvaggi, [arXiv:1307.6346].
- [27] A. Avetisyan *et al.* (2013), [arXiv:1307.XXXX].
- [28] R.M. Harris and S. Jain, *Eur. Phys. J. C* **72**, 2072 (2012) [arXiv:1112.4928].
- [29] J.Gao *et al.*, *Phys. Rev. D* **82**, 014020 (2010) [arXiv:1004.0876].
- [30] Y.L. Dokshitzer *et al.*, *JHEP* **9708**, 001 (1997) [hep-ph/9707323].
- [31] A. Caldwell, D. Kollar and K. Kröninger, *Comput. Phys. Commun.* **180**, 2197 (2009) [arXiv:0808.2552].
- [32] A. L. Fitzpatrick, J. Kaplan, L. Randall and L. T. Wang, *JHEP* **0709**, 013 (2007) [arXiv:hep-ph/0701150]; K. Agashe, H. Davoudiasl, G. Perez and A. Soni, *Phys. Rev. D* **76**, 036006 (2007) [arXiv:hep-ph/0701186]; O. Antipin, D. Atwood and A. Soni, *Phys. Lett. B* **666**, 155 (2008) [arXiv:0711.3175 [hep-ph]]; O. Antipin and A. Soni, *JHEP* **0810**, 018 (2008) [arXiv:0806.3427 [hep-ph]].
- [33] J. Alwall, M. Herquet, F. Maltoni, O. Mattelaer and T. Stelzer, *JHEP* **1106**, 128 (2011) [arXiv:1106.0522 [hep-ph]].
- [34] N. D. Christensen and C. Duhr, *Comput. Phys. Commun.* **180**, 1614 (2009) [arXiv:0806.4194 [hep-ph]].
- [35] T. Sjostrand, S. Mrenna and P. Z. Skands, *JHEP* **0605**, 026 (2006) [hep-ph/0603175].
- [36] M. Cacciari, G. P. Salam and G. Soyez, *JHEP* **04**, 063 (2008) [arXiv:0802.1189].
- [37] T. Junk, *Nucl. Instrum. Meth. A* **434**, 435 (1999) [hep-ex/9902006].
- [38] A. L. Read, *J. Phys. G* **28**, 2693 (2002).
- [39] K. Agashe, A. Belyaev, T. Krupovnickas, G. Perez and J. Virzi, *Phys. Rev. D* **77**, 015003 (2008) [arXiv:hep-ph/0612015].
- [40] S. D. Ellis, J. Huston, K. Hatakeyama, P. Loch and M. Tonnesmann, *Prog. Part. Nucl. Phys.* **60**, 484 (2008) [arXiv:0712.2447 [hep-ph]].
- [41] A. Abdesselam, E. B. Kuutmann, U. Bitenc, G. Brooijmans, J. Butterworth, P. Bruckman de Renstrom, D. Buarque Franzosi and R. Buckingham *et al.*, *Eur. Phys. J. C* **71**, 1661 (2011) [arXiv:1012.5412 [hep-ph]].
- [42] G. P. Salam, *Eur. Phys. J. C* **67**, 637 (2010) [arXiv:0906.1833 [hep-ph]].
- [43] P. Nath, B. D. Nelson, H. Davoudiasl, B. Dutta, D. Feldman, Z. Liu, T. Han and P. Langacker *et al.*, *Nucl. Phys. Proc. Suppl.* **200-202**, 185 (2010) [arXiv:1001.2693 [hep-ph]].

- [44] L. G. Almeida, R. Alon and M. Spannowsky, Eur. Phys. J. C **72**, 2113 (2012) [arXiv:1110.3684 [hep-ph]].
- [45] D. E. Soper and M. Spannowsky, Phys. Rev. D **87**, 054012 (2013) [arXiv:1211.3140 [hep-ph]].
- [46] D. E. Soper and M. Spannowsky, Phys. Rev. D **84**, 074002 (2011) [arXiv:1102.3480 [hep-ph]].
- [47] L. G. Almeida, S. J. Lee, G. Perez, G. Sterman and I. Sung, Phys. Rev. D **82**, 054034 (2010) [arXiv:1006.2035 [hep-ph]].
- [48] T. Plehn and M. Spannowsky, J. Phys. G **39**, 083001 (2012) [arXiv:1112.4441 [hep-ph]].
- [49] M. Backovic, J. Juknevich and G. Perez, JHEP **1307**, 114 (2013) [arXiv:1212.2977 [hep-ph]].
- [50] G. Aad *et al.* [ATLAS Collaboration], JHEP **1301**, 116 (2013) [arXiv:1211.2202 [hep-ex]].
- [51] M. Backovic, O. Gabizon, J. Juknevich, G. Perez, Y. Soreq, In preparation.
- [52] M. Backovic and J. Juknevich, arXiv:1212.2978.
- [53] P. M. Nadolsky, H. -L. Lai, Q. -H. Cao, J. Huston, J. Pumplin, D. Stump, W. -K. Tung and C. -P. Yuan, Phys. Rev. D **78**, 013004 (2008) [arXiv:0802.0007 [hep-ph]].
- [54] M. Cacciari, G. P. Salam and G. Soyez, JHEP **0804**, 063 (2008) [arXiv:0802.1189 [hep-ph]].
- [55] M. L. Mangano, M. Moretti, F. Piccinini and M. Treccani, JHEP **0701**, 013 (2007) [hep-ph/0611129].
- [56] K. Rehermann and B. Tweedie, JHEP **1103**, 059 (2011) [arXiv:1007.2221 [hep-ph]].
- [57] K. Agashe *et al.*, Phys. Rev. D **76**, 115015 (2007) [arXiv:0709.0007 [hep-ph]].
- [58] A. Belyaev, N. Christensen, A. Pukhov, Comput. Phys. Commun. **184**, 1729 (2013).
- [59] C. Dennis, M. Karagoz Unel, G. Servant and J. Tseng, arXiv:hep-ph/0701158; R. Contino and G. Servant, JHEP **0806**, 026 (2008) [arXiv:0801.1679 [hep-ph]].
- [60] Go to the link: http://www.snowmass2013.org/tiki-index.php?page=The+Path+Beyond+the+Standard+Model#Heavy_Fermions
- [61] M. Carena, A. D. Medina, B. Panes, N. R. Shah and C. E. M. Wagner, Phys. Rev. D **77**, 076003 (2008) [arXiv:0712.0095 [hep-ph]].
- [62] A. Juste, Y. Kiyo, F. Petriello, T. Teubner, K. Agashe, P. Batra, U. Baur and C. F. Berger *et al.*, hep-ph/0601112.
- [63] K. Agashe and R. Contino, Phys. Rev. D **80**, 075016 (2009) [arXiv:0906.1542 [hep-ph]]; A. Azatov, M. Toharia and L. Zhu, Phys. Rev. D **80**, 035016 (2009) [arXiv:0906.1990 [hep-ph]].
- [64] A. Azatov, M. Toharia, L. Zhu Phys. Rev. D **82**, 056004 (2010) [arXiv:1006.5939 [hep-ph]].
- [65] A. Falkowski, Phys. Rev. D **77**, 055018 (2008) [arXiv:0711.0828 [hep-ph]].

- [66] M. S. Carena, E. Ponton, T. M. P. Tait, C. E. M. Wagner Phys. Rev. D **67**, 096006 (2003) [hep-ph/0212307].
- [67] J. A. Cabrer, G. von Gersdorff, M. Quiros JHEP **1201**, 033 (2012) [arXiv:1110.3324 [hep-ph]].
- [68] H. Davoudiasl, G. Perez, A. Soni Phys. Lett. B **665**, 67 (2008) [arXiv:0802.0203 [hep-ph]].
- [69] E. Ponton, L. Randall JHEP **0904**, 080 (2009) [arXiv:0811.1029 [hep-ph]].
- [70] K. Agashe, D. Kim, M. Toharia, D. G. E. Walker Phys. Rev. D **82**, 015007 (2010) [arXiv:1003.0899 [hep-ph]]; K. Agashe, D. Kim, D. G. E. Walker, L. Zhu Phys. Rev. D **84**, 055020 (2011) [arXiv:1012.4460 [hep-ph]].
F. D'Eramo, M. McCullough, J. Thaler arXiv:1210.7817 [hep-ph]; G. Belanger, K. Kannike, A. Pukhov, M. Raidal JCAP **1301**, 022 (2013) [arXiv:1211.1014 [hep-ph]].
- [71] K. Agashe, A. Azatov, T. Han, Y. Li, Z. -G. Si, L. Zhu Phys. Rev. D **81**, 096002 (2010) [arXiv:0911.0059 [hep-ph]].